The Study of Strongly Correlated Electronic Systems Using Dynamical Mean Field Theory

by

Tesfaye Mamuye Mulatu

A dissertation submitted to
the Department of Physics of Addis Ababa University
in partial fulfillment of the requirements

for the Degree of Doctor of Philosophy
in Condesed Matter Physics

Addis Ababa, Ethiopia June 2016

I would like to dedicate this thesis to my Mother & to my uncle Talargachew Melese

Declaration

I hereby declare that except where specific reference is made to the work of others, the contents of this dissertation are original and have not been submitted in whole or in part for consideration for any other degree or qualification in this, or any other University. This dissertation is the result of my own work and that all sources of material used for the dissertation have been duly acknowledged.

Name: Tesfaye Mamuye Mulatu

Signature: _____

Date: _____

This PhD dissertation has been submitted for examination with my approval as university advisor.

Advisor's Name: Prof. P. Singh

Signature: _____

Date: _____

Addis Ababa University
Department of Physics

The Study of Strongly Correlated Electronic Systems Using Dynamical Mean Field Theory

by

Tesfaye Mamuye Mulatu

Approved by the Examination Committee

	Signature	Date
Prof. Keya Dharamvir, External Examiner:	_____	_____
Dr. Chernet Amente, Internal Examiner:	_____	_____
Prof. P. Singh, Thesis Advisor:	_____	_____
Dr. Teshome Senbeta, Chairman:	_____	_____

Acknowledgements

I would thank my advisor Prof. P. Singh for his guidence, patience , giving me the freedom to do things the way I wanted and the trust he put into me and my abilities. I appreciated him for for his friendly approach, limitless and invaluable encouragement without any reservation during the whole period of the research work.

I would also like to thank Dr. Teshome Senbeta head of the department of physics, W/o Tsilat Adinew (secretary) and physics department community for their contribution to the completion of my work.

My especial thanks goes to Gemechu Fanta for installing the software I used for my work.

Last but not least, it gives me great pleasure to thank Ambo Univerity for their help in sponsoring.

Abstract

The physics of strongly correlated electronic systems has attracted much attention because of its unique and distinct properties like Mott metal-to-insulator transition, giant magneto-resistance, superconductivity. While the density functional theory (DFT), the standard approach to electronic band calculations, is able to describe properties of weakly correlated systems but is known to have serious limitation in the description of strongly correlated systems, the dynamical mean field theory (DMFT) has become an established method for the treatment of strongly correlated systems. In this dissertation, we study the properties of correlated electronic systems near Mott metal-to-insulator transitions using DMFT, which maps Hubbard like lattice model in infinite coordination number to a single site impurity Anderson model with the self-consistent conditions. We implement the continuous-time hybridization expansion (CT-HYB) version of continuous-time quantum Monte Carlo (CT-QMC) for the impurity model to investigate the Mott metal-to-insulator in the Hubbard model on Bethe lattice without symmetry braking. At half filling a gap opening transition is found to occur as the interaction strength is increased beyond critical value. We extend our analysis to the inclusion of retarded interaction (electron-phonon interaction) in the frame work of Hubbard-Holstein model. We implement the CT-HYB in the presence of retarded interaction for the impurity model. The effect of the inclusion of retarded interaction to Hubbard model is to shift the Mott metal-to-insulator to a large critical values as compared to the pure Hubbard model. The interplay of electron-electron and electron-phonon interaction near the Mott metal-to-insulator transition are discussed.

Table of contents

List of figures

Chapter 1

Introduction

The fundamental laws of condensed matter physics have been essentially known since the advent of quantum mechanics in the first half of the last century. Apart from relativistic effects, the physical properties of any materials [1] are determined by the solution of the Schrödinger equation $\mathcal{H}\psi = E\psi$ with the Hamiltonian

$$\mathcal{H} = -\sum_{\alpha} \frac{\hbar^2}{2M_\alpha}\nabla_\alpha^2 + \frac{1}{2}\sum_{\alpha\neq\alpha'} \frac{Z_\alpha Z_{\alpha'} e^2}{|\mathbf{R}_\alpha - \mathbf{R}_{\alpha'}|} - \sum_{j} \frac{\hbar^2}{2m_e}\nabla_j^2 - \sum_{j,\alpha} \frac{Z_\alpha e^2}{|\mathbf{r}_j - \mathbf{R}_\alpha|} + \frac{1}{2}\sum_{j\neq j'} \frac{e^2}{|\mathbf{r}_j - \mathbf{r}_{j'}|} \tag{1.1}$$

of the material under consideration. Here, $\{\mathbf{r}_j\}$ are the position of the N_e electrons, $\{\mathbf{R}_\alpha\}$ those of the N_n nuclei, Z_α the atomic numbers, and M_α the nuclear masses. Using the fact that the mass of any nucleus is much larger than the electron mass, the Born-Oppenheirmer approximation (BOA) allows to separate the dynamics of the nuclei from that of the electrons.One can thus reduce the problem to the electronic problem only by the electronic Hamiltonian

$$H = -\sum_{j} \frac{\hbar^2}{2m_e}\nabla_j - \sum_{j,\alpha} \frac{Z_\alpha e^2}{|\mathbf{r}_j - \mathbf{R}_\alpha|} + \frac{1}{2}\sum_{j\neq j'} \frac{e^2}{|\mathbf{r}_j - \mathbf{r}_{j'}|}. \tag{1.2}$$

The periodic lattice potential $\sum_{j,\alpha} \frac{Z_\alpha e^2}{|\mathbf{r}_j - \mathbf{R}_\alpha|}$ is then often denoted as external potential $V(\mathbf{r})$, to highlight the electronic system character. The remaining part of $\mathcal{H}$ eventually

leads to phonon excitation and their interactions (see eq. 1.5), the electron-phonon coupling, *i.e.*, physics beyond the BOA [2].

Since the development of quantum mechanics many successful approximations to eq.(1.2) have been developed. One of the most prominent approximation is the density functional theory (DFT), which is free of parameters and allows calculations based on first principles (ab-initio), for which its main creator, Walter Kohn, was recognized with 1998 Noble prize in chemistry [3]. It relies on the Hohenberg-Kohn theorems [4, 5] which establish the electronic density $n(\mathbf{r})$ as the basic variable instead of the electronic wave function $\psi(\mathbf{r}_1, \cdots, \mathbf{r}_N)$. One could then compute the ground state energy of a system without the knowledge of the full many-body wave-function. This implies a tremendous reduction from a problem involving N-body wave-function with 3N-coordinates to density $n(\mathbf{r})$ with merely three variables. Thus instead of directly solving the many-body Schrödinger equation, the solution of mapping of the system onto three dimensional density is sufficient.

In materials where correlations of electrons are weak, (DFT) and the local density approximation (LDA) are very successful and manage to predict experimental properties like the band structure of real materials to high accuracy. However, DFT method are not accurate enough when applied to strongly correlated materials. Prominent examples are, transition metal system like NiO, which is experimentally an insulator with band gap of 4.3eV [6], but is predicted to be a metal by DFT [7].

The physics of materials with strongly correlated electrons is one of the most exciting topics of present-day theoretical and experimental solid-state research. A wide variety of interesting phenomena can be attributed to electronic correlations, among them Mott metal-insulator transitions, the giant magneto-resistance (Noble price 2007, Fert and Grünberg), and superconductivity.

The essential physics of strongly correlated electrons can be captured in effective low energy models, which are, however, still complicated many-body problems. One of the possible simplifications is the mapping of the continuum problem (Eq. 1.1)

onto a lattice model that consists of a truncated number of basis states. In second quantization, the resulting Hamiltonian reads

$$H = -\sum_{ij} t_{ij} d^{\dagger}_{i,\sigma} d_{j,\sigma} + \frac{1}{2} \sum_{ijkl,\sigma,\sigma'} V_{ijkl} d^{\dagger}_{j,\sigma} d^{\dagger}_{k,\sigma'} d_{l,\sigma'} d_{j,\sigma} \tag{1.3}$$

where the creation (annihilation) operators $d^{\dagger}_{i,\sigma}$ ($d_{i,\sigma}$) creates (annihilates) an electron with spin σ at site i. Besides the limitation to a truncated basis set, we can further limit the interaction terms V we allow in Eqn. (1.3). One popular choice that is often considered is the so-called Hubbard model [8], where only the largest contributions of (Eq. 1.3) are kept. V_{ijkl} is restricted to the on-site Coulomb repulsion V_{iiii} = U and t_{ij} to purely nearest neighbor hopping, with $n_{i\sigma} = d^{\dagger}_{i\sigma} d_{i\sigma}$:

$$H = -\sum_{\langle ij \rangle,\sigma} t_{ij} (d^{\dagger}_{i\sigma} d_{j\sigma} + d^{\dagger}_{j\sigma} d_{i\sigma}) + U \sum_{i} n_{i\uparrow} n_{i\downarrow}. \tag{1.4}$$

The exotic properties and complex phase diagram of strongly correlated materials result from competing interaction terms in their Hamiltonians. Thus, Mott-Hubbard metal-insulator transition [9, 10], one of the central topics of the strongly correlated field, originates from the competition between tendencies of the correlated electrons to delocalize due to their kinetic energy and localize due to the Coulomb interaction between them. The tendency to delocalize leads to the band formation and in the limiting case has a simple description in momentum space. On the other hand, tendency to localize leads to atomic-like behavior which is well described in real space. The crossover is difficult to treat theoretically even on the level of models since the electron kinetic energy and interaction energy are of the same order of magnitude and is impossible to develop perturbation theory around either metallic or atomic limits.

For materials where electron-phonon coupling is significant the BOA breaks down. Then there is the possibility to formulate a simplified Fröhlich Hamiltonian in real

space using further only Einstein phonons, the so-called Holstein Hamiltonian [27]

$$H_{hol} = -\sum_{\langle ij\rangle,\sigma} t_{ij}(d^{\dagger}_{i\sigma}d_{j\sigma} + d^{\dagger}_{j\sigma}d_{i\sigma}) + \lambda\sum_{i}(b^{\dagger}_{i} + b_n)(n_{i\uparrow} + n_{i\downarrow} - 1) + \omega_0\sum_{i} b^{\dagger}_{i}b_i \qquad (1.5)$$

where $b^{\dagger}$/ b are bosonic creation/annihilation operators for the phonons, ω_0 the Einstein-mode frequency and λ the electron-phonon coupling strength.

Starting in 1990s, dynamical mean field theory (DMFT) [11] emerges as a prominent methods to study the Hubbard-like models, which can, for example quantitatively describe the Mott transition. It is based on a mapping of the lattice model onto a self-consistent quantum impurity problem, an approximation which becomes exact in the limit of infinite dimensions. The major challenge in the practical application of the DMFT approach is the solution of the self-consistent quantum impurity problem, which is, although simpler than the original lattice model, still a complicated many-body model. From the invention of the DMFT approach, the Hirsch-Fye Quantum Monte Carlo algorithm [12] has become the standard QMC method for the solution of the DMFT impurity problem. Recently a continuous- time Quantum Monte Carlo (CT-QMC) impurity solvers [13–15] has been developed which overcome some of the limitation of the Hirsch-Fye algorithm. In this thesis we use the continuous-time hybridization expansion (CT-HYB) version of CT-QMC.

This thesis is outlined as follows. In chapter 2, we introduce Hubbard model, Hubbard model supplemented by a Holstein coupling term also called Hubbard- Holstein model and the Mott metal-insulator transition. This is followed by a presentation of DMFT equations, illustrating how a lattice model, in infinite dimension, can be mapped to a single-site quantum impurity problem (single-impurity Anderson model (SIAM)) embedded in an effective medium. Solving the SIAM to obtain dynamical quantities requires the implementation of impurity solver. A numerically exact impurity solver of SIAM, the Continuous time quantum Monte Carlo is then presented in chapter 3. Numerical results for Hubbard and Hubbard-Holstein model are presented in chapter 4 and chapter 5 respectively. We end in chapter 6 with conclusions.

Chapter 2

Model Hamiltonians and Dynamical Mean-Field Theory

2.1 Hubbard Model

The model proposed by Gutzwiller [16], Hubbard [8] and Kanamori [17] in 1963, commonly referred to as the Hubbard model, is one of the most widely studied quantum lattice models in theoretical physics [18]. It can be stated in second quantized form as follows

$$H = \sum_{i,j\sigma} t_{ij}(d^{\dagger}_{i\sigma} d_{j\sigma} + hc) + U \sum_{i} n_{i\uparrow} n_{i\downarrow}. \tag{2.1}$$

where t_{ij} is the hopping amplitude, U is the local Hubbard interaction, $d^{\dagger}_{i\sigma}(d_{i\sigma})$ is the creation (annihilation) operator of an electron with spin σ in a Wannier orbital localized at lattice site i, and $n_{i\sigma} = d^{\dagger}_{i\sigma} d_{i\sigma}$ is particle number operator on site i. Apart from the physical parameters t_{ij} and U, there are other implicit "parameters" for the model, such as the lattice type (e.g., square, triangular, fcc, etc.), the filling n (n-number of electron per lattice site/ orbital) and the temperature.

The above introduced Hubbard model is the simplest model of correlated electronic system and, solved analytically in one-dimension using Bethe ansatz [19], showing that

at half-filling case the system is insulating for $U > 0$, being metallic at $U = 0$. This fact makes the employment of various approximations unavoidable. To be confident that some particular approximation at hand is a meaningful one, it is important to explore the different limiting situations in which the original model reduces to a simpler one and some reliable results can be obtained. Some of the limiting cases are:

Non-interacting limit U=0. Non-interacting particles, with Hamiltonian $H - \mu N = \sum_{\mathbf{k}\sigma}(\epsilon_{\mathbf{k}} - \mu)c^{\dagger}_{\mathbf{k}\sigma}c_{\mathbf{k}\sigma}$, are characterized by the non-interacting Green's function $G_{\mathbf{k}\sigma}$ and non-interacting density of state $\rho(\epsilon)$ [20] [1]

$$G_{\mathbf{k}}(i\omega) = \frac{1}{i\omega_n - \epsilon_{\mathbf{k}} + \mu}, \qquad \rho(\omega) = \frac{1}{L}\sum_{\mathbf{k}}\delta(\omega - \epsilon_{\mathbf{k}}), \tag{2.2}$$

which is the familiar electronic density of states (DOS) from single-particle theory for the band dispersion $\epsilon_{\mathbf{k}}$.

Atomic limit t=0. In the absence of hopping, each atom has four eigenstates: $|0\rangle, |\uparrow\rangle, |\downarrow\rangle$, and $|\uparrow\downarrow\rangle$ with energies 0, $-\mu$, $-\mu$ and $U - 2\mu$, respectively. In this case, $H_{at} = U\sum_i n_{i\uparrow}n_{i\downarrow} - \mu\sum_{i\sigma} n_{i\sigma}$ is the atomic Hamiltonian, $-\mu = \epsilon_0$ plays the role of the one-electron energy of that single-level atom and, the partition function $Z = Tr(e^{-\beta H}) = 1 + 2e^{\beta\mu} + e^{-\beta(U-2\mu)}$, where $\beta = \frac{1}{T}$. In principle, once the partition function is known, we can determine properties like the fillings, double occupancy, total energy, local moment, the single particle Green's function, etc. The Green's function in imaginary time read,

$$G_{\sigma}(\tau - \tau') \;=\; -\langle T_{\tau} d_{\sigma}(\tau) d^{\dagger}_{\sigma}(\tau')\rangle = -\frac{1}{Z} Tr\left[e^{-\beta H} T_{\tau}(d_{\sigma}(\tau) d^{\dagger}_{\sigma}(\tau'))\right] \tag{2.3}$$

where T_{τ} is the time ordering operator and the operators are ordered such that $T_{\tau}(d_{\sigma}(\tau)d^{\dagger}_{\sigma}(\tau'))$ is equal to $d_{\sigma}(\tau)d^{\dagger}_{\sigma}(\tau')$ for $\tau > \tau'$ and $d^{\dagger}_{\sigma}(\tau')d_{\sigma}(\tau)$ when $\tau' > \tau$. For

[1] L number of lattice site

τ'=0, equation (2.3) becomes

$$G_\sigma(\tau) = -\frac{1}{Z}\left[e^{-\beta H} d_\sigma(\tau) d_\sigma^\dagger\right]. \tag{2.4}$$

With the help of the Heisenberg operator definition, we have

$$\begin{aligned} G_\uparrow(\tau) &= -\frac{1}{Z} Tr\left[e^{-\beta H} d_\uparrow(\tau) d_\uparrow^\dagger\right] = -\frac{1}{Z} Tr\left[e^{-(\beta-\tau)H} d_\uparrow e^{-H\tau} d_\uparrow^\dagger\right] \\ &= -\frac{e^{\mu\tau} + e^{\mu(\beta-\tau)} e^{-\tau(U-2\mu)}}{1 + 2e^{\beta\mu} + e^{\beta(2\mu-U)}} \end{aligned} \tag{2.5}$$

The corresponding frequency Green's function can be obtained by Fourier Transform

$$G_\uparrow(i\omega_n) = \int_0^\beta d\tau e^{i\omega_n\tau} G_\uparrow(\tau) = \frac{1}{Z}\left[\frac{1 + e^{\beta\mu}}{i\omega_n + \mu} + \frac{e^{\beta\mu} + e^{-\beta(U-2\mu)}}{i\omega_n + \mu - U}\right] \tag{2.6}$$

Note that $(1 + e^{\beta\mu})/Z = 1 - \langle n_\uparrow\rangle$, $(e^{\beta\mu} + e^{-\beta(U-2\mu)})/Z = \langle n_\uparrow\rangle$, so the imaginary Matsubara Green's function with spin-σ can be further written as

$$G_\sigma(i\omega_n) = \frac{1 - \langle n_\sigma\rangle}{i\omega_n + \mu} + \frac{\langle n_\sigma\rangle}{i\omega_n + \mu - U} = \frac{1 - \langle n_\sigma\rangle}{i\omega_n + U/2} + \frac{\langle n_\sigma\rangle}{i\omega_n - U/2} \tag{2.7}$$

At half filling $\langle n\rangle = 1$, and $\langle n_\uparrow\rangle = \langle n_\downarrow\rangle = 1/2$, the spectral function can be obtained from the Matsubara Green function by the analytic continuation[2] from $i\omega_n$ to $\omega + i0^+$ *i.e.*,

$$G(\omega + i0^+) = \frac{1}{2}[\mathcal{P}\frac{1}{\omega + U/2} + \mathcal{P}\frac{1}{\omega - U/2} - i\pi[\delta(\omega + U/2) + \delta(\omega - U/2)]] \tag{2.8}$$

so the spectral function is

$$A(\omega) = -\frac{1}{\pi} ImG(\omega + i0^+) = \frac{1}{2}\left[\delta(\omega + \frac{U}{2}) + \delta(\omega - \frac{U}{2})\right]. \tag{2.9}$$

[2] Applying the Dirac identity, $\lim_{\eta\to 0}\frac{1}{\omega \pm i\eta} = \mathcal{P}\frac{1}{\omega} \mp i\pi\delta(\omega)$.

which corresponds to a spectral function with two δ peaks separated by an energy U, and for half-filling the system is insulating. As the low energy δ peak only have contributions from singly occupied states the double occupancy is zero for half-fillings.

Large U limit. This limit case is not exactly solvable but it leads to a model that can be treated more easily. At half-filling, the Hubbard model (2.1) is reduced to an anti-ferromagnetic Heisenberg model up to the second order in t/U [21]

$$H = \sum_{ij} J\mathbf{S}_i\mathbf{S}_j, \qquad J = \frac{4t^2}{U} > 0 \tag{2.10}$$

with the spin operators $\mathbf{S}$ at site i and j. Away from half-filling, we obtain the $t-J$-model which was first derived by Spalek in 1988 [22].

2.2 Hubbard-Holstein model

A strongly correlated system coupled to phonon can be described through the Hubbard model supplemented by a Holstein coupling term (retarded interaction). This is called Hubbard-Holstein model. We can write the single orbital Hubbard model with retarded interactions as

$$H = \sum_{\langle i,j\rangle\sigma} t_{ij}[d^\dagger_{i\sigma}d_{j\sigma} + d_{i\sigma}d^\dagger_{j\sigma}] - \mu\sum_i[n_{i\uparrow} + n_{i\downarrow}] + U\sum_i n_{i\uparrow}n_{i\downarrow} + H_{ret}. \tag{2.11}$$

The retarded interaction term H_{ret} reads

$$H_{ret} = \lambda\sum_i(b^\dagger_i + b_i)(n_{i\uparrow} + n_{i\downarrow} - 1) + \omega_0\sum_i b^\dagger_i b_i, \tag{2.12}$$

where $b^\dagger_i$ is a creation operator of a phonon, λ is the coupling constant between electrons and phonons and ω_0 is the phonon frequency.

The Hubbard-Holstein model represents an ideal playground where the interplay between the repulsive Hubbard interaction and the retarded attractive one mediated by

phonon can be studied, evidencing the non-trivial effects coming from their competition. Our study focuses on the paramagnetic and non-superconducting sector of the Hubbard-Holstein model, where the interesting physics of the transition between the metal and the Mott insulator emerges, not hidden by broken-symmetry phases.

2.3 The Mott Metal-Insulator transition

From the above limiting cases of the Hubbard model (2.1), one can presume the existence of a metal-insulator transition in the intermediate parameter range. Since (2.1) consists of hopping hampered only by Coulomb repulsion, this presumed transition is caused by quantum fluctuations. Such a transition has been proposed by Mott [23] fourteen years before the introduction of the Hubbard model in 1963, to argue that the observation of insulator in transition mono-oxides with partially filled $3d$ band such as NiO, MnO, or CoO by de Boer and Verwey [24], is due to the strong electron-electron repulsion that prohibits double occupancy in each energy state, the result is that each site is singly occupied, any electron hopping, if occurring, would cost a large amount of energy of the order of the on-site Coulomb interaction. This correlation- induced metal-insulator transition does not break translational invariance and is called the Mott transition, as it was originally put forward by Mott [23].

Making use of the half-filled, single-band Hubbard model (2.1) the Mott–transition was studied intensively in the past[11]. Important early results were obtained by Hubbard [8] within a Green function decoupling scheme, and by Brinkman and Rice [25] within the Gutzwiller variational method [4], both at $T = 0$.

Hubbard starts with the paramagnetic insulating phase where the spectral density has split in to an upper and a lower Hubbard band. Between both bands there exists an energy gap $\Delta = U - 2D$. If U is lowered, the gap becomes smaller and at a certain critical interaction value U_{c1} both bands touch each other (*i.e* the gap closes) and a transition to metallic phase occurs. However, this picture cannot describe the Fermi-liquid behavior of the metallic phase. By contrast, Brinkman and Rice [25] started

with the metallic phase and gives a good description of the low-energy, quasi-particle behavior. The ratio between the effective mass m^* of the quasi-particle and the electron mass m defines the quasi-particle weight Z via

$$\frac{1}{Z} = \frac{m^*}{m}. \tag{2.13}$$

The Fermi energy ϵ_F is also renormalized by Z, *i.e.*, $\epsilon_F^* \sim Z\epsilon_F \sim ZD$ (D the half-band width, also equal to the Fermi energy of the non-interacting system at half-filling), which can be interpreted as the coherence-scale for quasi-particles. At a certain critical Coulomb repulsion U_{c2}, the quasi-particle weight vanishes ($\frac{1}{Z} \propto \frac{1}{U_{c2}-U} \longrightarrow \infty$) and hence the divergence of the quasi-particle effective mass. This defines the transition to the insulating phase.

The Brinkman-Rice-scenario adequately describes the low energy behavior, however, cannot address high-energy features like the Hubbard bands of the correlated metals. An important achievement of dynamical mean field theory (DMFT) is the ability to describe both types of excitations on an equal footing. The actual spectrum of a correlated metal has three salient spectral features lower and upper Hubbard-bands at high energy, and a narrowed density of states corresponding to quasi-particle excitations at low energy

2.4 Dynamical Mean Field Theory

As we mentioned in section (2.1), the Hubbard model, even in its simplest one-orbital band form, is impossible to solve analytically, thus one would typically think of a perturbation approach. This would be either to perform an expansion around the atomic limit in t or to perform an expansion around the noninteracting limit in U. If we follow one of these approaches we miss the most interesting regime where the two parameters are of similar order and where the physics of strongly correlated metallic systems and the Mott-Hubbard metal insulator transition happen.

Metzner and Vollhardt [26] introduced a new limit to correlated electron systems, the limit of infinite dimensions $d \to \infty$ or equivalently an infinite number of neighboring lattice sites. This approach retained the competition between kinetic energy t and Coulomb interaction U of electrons while resulting in a simplified, momentum-independent self-energy: $\Sigma_{\mathbf{k}}(\omega) \xrightarrow{d\to\infty} \Sigma(\omega)$. Soon after the publication of the work by Metzner and Vollhardt [26], Müller-Hartmann [27, 28] showed that only the local Coulomb interaction yields dynamic (frequency dependent self-energies) whereas the non-local density-density interactions are reduced to their Hartree term. This is the foundation of the dynamical mean-field theory (DMFT) developed by Georges and Kotliar [29], who showed that a many-body model like the Hubbard model is mapped onto the self-consistent solution of an auxiliary Anderson impurity model for $d \to \infty$.

2.4.1 Proper scaling in the limit infinite dimension

We consider the kinetic energy term (2.1) since the interaction term U is purely local is independent of lattice structure and dimension. For hopping between nearest-neighbor sites i and j with amplitude $t_{ij} = -t$ on a d-dimensional hypercubic lattice the dispersion $\epsilon_{\mathbf{k}}$ is given by[3]

$$\epsilon_{\mathbf{k}} = -2t \sum_{i=1}^{d} \cos k_i. \tag{2.14}$$

The density of states (DOS) corresponding to $\epsilon_{\mathbf{k}}$ is

$$N_d = \sum_{\mathbf{k}} \delta(\omega - \epsilon_{\mathbf{k}}). \tag{2.15}$$

This is simply the probability density for finding $\omega = \epsilon_{\mathbf{k}}$ for a random choice of $\mathbf{k} = (k_1, \cdots, k_d)$. If the k_i are chosen randomly, $\epsilon_{\mathbf{k}}$ in (2.14) is the sum of (independent) random numbers $-2t \cos k_i$. The central limit theorem then implies that in the limit

[3] we set Planck's constant $\hbar$, Boltzmann's constant k_B, and the lattice spacing equal to unity.

$d \to \infty$ the DOS is given by a Gaussian

$$N_d(\omega) \xrightarrow{d\to\infty} \frac{1}{2t\sqrt{\pi d}} exp\left[-\left(\frac{\omega}{2t\sqrt{d}}\right)^2\right]. \tag{2.16}$$

Unless t is scaled properly with d this density of states will become arbitrarily broad and featureless for $d \to \infty$. Clearly only the scaling

$$t \to \frac{t^*}{\sqrt{d}}, \qquad t^* = const., \tag{2.17}$$

yields a non-trivial limit $d \to \infty$ for the density of state [26]. In analogy to eq. (2.17), the scaling for general lattice sites i and j, can be expressed in terms of $d^{||\mathbf{R}_i - \mathbf{R}_j||}$ where $||\mathbf{R}_i - \mathbf{R}_j||$ denotes the distance from site i to site j in a suitable metric [4]

$$t_{ij} \longrightarrow \frac{t^*_{ij}}{d^{\frac{1}{2}\|\mathbf{R}_i - \mathbf{R}_j\|}}. \tag{2.18}$$

And for general sites i and j the single particle Green's function scales as [20, 30]

$$G_{ij}(\omega) \sim \frac{1}{d^{\frac{1}{2}\|\mathbf{R}_i - \mathbf{R}_j\|}}. \tag{2.19}$$

With the scaling (2.19), the kinetic energy per site scales properly, *i.e*, it stays finite. To see this note that there are $d^{\|\mathbf{R}_i - \mathbf{R}_j\|}$ terms in the sum for every class of equivalent site j. This factor is, however, canceled by a factor $d^{-\frac{1}{2}\|\mathbf{R}_i - \mathbf{R}_j\|}$ for t_{ij} and another factor $d^{-\frac{1}{2}\|\mathbf{R}_i - \mathbf{R}_j\|}$ for $\langle \hat{d}^\dagger_{i\sigma} \hat{d}_{j\sigma} \rangle$.

2.4.2 Local Self energy

How do the skeleton diagrams scales with d? If there are two sites $i \neq j$, both sites have to be connected by three Green's functions, which follows directly from the definition of skeleton diagrams[30]. Let us hold i fixed for the moment. We now compare the

[4] Example, in the hypercubic lattice, $||\mathbf{R}_i - \mathbf{R}_j||$, the so-called Manhattan metric which gives the smallest number of lattice steps between site i and j

case $j \neq i$ with case $j = i$. Suppose $j \neq i$. The three Green's functions lines can thus contribute at most $\mathcal{O}(d^{-\frac{3}{2}\|\mathbf{R}_i - \mathbf{R}_j\|})$. The summation over j will then yield an order $\mathcal{O}(d^{\|\mathbf{R}_i - \mathbf{R}_j})$. As a consequence, any skeleton diagram is suppressed at least by a factor $\mathcal{O}(d^{-\frac{1}{2}\|\mathbf{R}_i - \mathbf{R}_j\|})$, which become irrelevant for $d \longrightarrow \infty$. By contrast, for $j = i$ the Green's function are of the order $\mathcal{O}(d^0)$, and there is no summation. Consequently, all the skeleton diagrams are purely local. As a result, the self energy itself becomes a purely local (site diagonal) [26], but retains its dynamics [27]

$$\Sigma_{ij\sigma}(\omega) = \delta_{ij}\Sigma_{ii\sigma}(\omega) = \delta_{ij}\Sigma_{\sigma}(\omega). \tag{2.20}$$

In the paramagnetic phase we may write $\Sigma_{ii\sigma}(\omega) = \Sigma(\omega)$. The Fourier transform of $\Sigma_{ij\sigma}$ is then momentum-independent, *i.e.*, $\Sigma_{\mathbf{k}\sigma}(\omega) = \Sigma_{\sigma}(\omega)$.

That allows to reduce the problem of electron on the lattice in Hubbard model to single-site (local) problem. The lattice problem is hence reduced to a local problem: an electron may still leave the site i, interact on other sites -thereby being dressed by some self energy Σ -and return to site i at a later time, but this is fully described by the local interacting Green's function containing the self energy. The other sites can thus be viewed as a bath which is described by a propagator and a self energy without the need to distinguish the other sites anymore. Only on the local site i, the full interacting many body problem has to be solved.

The momentum-independence of the self energy has immediate consequences for the lattice Green's function which then can be written as

$$G_{\mathbf{k}}(i\omega) = \frac{1}{i\omega + \mu - \epsilon_{\mathbf{k}} - \Sigma(i\omega)}, \tag{2.21}$$

with chemical potential μ, and $\epsilon_{\mathbf{k}}$ is the Fourier transform of the hopping integral, *i.e*, the dispersion relation of non-interacting tight-binding band:

$$\epsilon_{\mathbf{k}} = \sum_{ij} t_{ij} e^{i\mathbf{k}.(\mathbf{R}_i - \mathbf{R}_j)},$$

the local Green's function takes the form

$$G_\sigma(i\omega) = \sum_{\mathbf{k}} G_{\mathbf{k}\sigma}(i\omega) = \int_{-\infty}^{\infty} \frac{d\epsilon \rho(\epsilon)}{i\omega + \mu - \epsilon - \Sigma_\sigma(i\omega)}, \tag{2.22}$$

with $\rho(\epsilon)$ being the density of the non-interacting density of states. Notice that the lattice structure enters into the local Green's function only via $\rho(\epsilon)$.

2.4.3 Derivation of effective single-site action

The derivation presented here will be borrowed from classical statistical mechanics, where it is known under the name "cavity method". The underlying idea is to focus on a given site of the lattice, say $i = 0$, and to explicitly integrate out the degrees of freedom on all other lattice sites in order to define an effective dynamics for the selected site [29]. It will be assumed in this section, for simplicity, that no symmetry breaking occurs and we are dealing with translational invariant paramagnetic phase

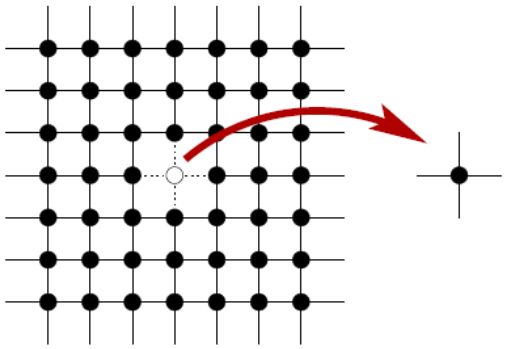

Fig. 2.1 Cavity created in the lattice by removing a single site and its adjacent bonds.

The partition function for Hubbard model (eq. 2.1) can be written as a functional integral over the Grassmann variables[31] [for detail see Appendix B]:

$$Z = \int \prod_{i\sigma} Dc^*_{i\sigma} Dc_{i\sigma} e^{-S}, \tag{2.23}$$

with the action

$$\begin{aligned} S &= \int_0^\beta d\tau \left[\sum_{i,\sigma} c^*_{i\sigma}(\tau) \left(\frac{\partial}{\partial \tau} - \mu \right) c_{i\sigma}(\tau) + H(c^*_{i\sigma}, c_{i\sigma}(\tau) \right] \\ &= \int_0^\beta d\tau \left[\sum_{i,\sigma} c^*_{i\sigma}(\tau) \left(\frac{\partial}{\partial \tau} - \mu \right) c_{i\sigma}(\tau) - \sum_{i,j,\sigma} t_{ij} c^*_{i\sigma}(\tau) c_{j\sigma}(\tau) + \sum_i U n_{i\uparrow}(\tau) n_{i\downarrow}(\tau) \right]. \end{aligned} \tag{2.24}$$

Following up on the idea of a classical mean field theory, one would like to reduce this to an effective single-site action S_{eff} defined by

$$\frac{1}{Z_{eff}} e^{-S_{eff}} = \frac{1}{Z} \int \prod_{i \neq 0, \sigma} D c^*_{i\sigma} D c_{i\sigma} e^{-S}. \tag{2.25}$$

Therefore, we want to integrate out the contribution from all sites $i \neq 0$ and keep the full dynamics for site 0. In order to achieve this, let us rewrite the action as the sum of three terms $S = S_0 + \Delta S + S^0$, where

$$S_0 = \int_0^\beta d\tau \left[\sum_\sigma c_{0\sigma}(\tau) \left(\frac{\partial}{\partial \tau} - \mu \right) c_{0\sigma}(\tau) + U n_{0\uparrow}(\tau) n_{0\downarrow}(\tau) \right],$$

$$\Delta S = - \int_0^\beta d\tau \left[\sum_{i\sigma} t_{i0} c^*_{i\sigma}(\tau) c_{0\sigma}(\tau) + t_{0i} c_{0\sigma}(\tau) c_{i\sigma}(\tau) \right],$$

and

$$S^{(0)} = \int_0^\beta d\tau \left[\sum_{i \neq 0, \sigma} c^*_{i\sigma}(\tau) \left(\frac{\partial}{\partial \tau} - \mu \right) c_{0\sigma}(\tau) - \sum_{i,j \neq 0, \sigma} t_{ij} c^*_{i\sigma}(\tau) c_{j\sigma}(\tau) + \sum_{i \neq 0} U n_{i\uparrow}(\tau) n_{i\downarrow}(\tau) \right].$$

S_0 is the action of the site 0, decoupled from the rest of the lattice. $S^{(0)}$ is the action of the lattice with the site 0 removed. ΔS is the action connecting the site 0 with the lattice. With these definitions, the partition function can be written as

$$Z = \int D c^*_{0\sigma} D c_{0\sigma} e^{-S_0} \int \prod_{i \neq 0} D c^*_{i\sigma} D c_{i\sigma} e^{-S^{(0)} - \Delta S} \tag{2.26}$$

and use the ensemble average

$$\langle X\rangle^{(0)} = \frac{1}{Z^{(0)}}\int \prod_{i\neq 0,\sigma} Dc^*_{i\sigma}Dc_{i\sigma}Xexp[-S^{(0)}] \tag{2.27}$$

taken with respect to $S^{(0)}$, with $Z^{(0)}$ being the corresponding partition function. With these the corresponding partition function reads

$$\begin{aligned} Z &= Z^{(0)}\int Dc^*_{0\sigma}Dc_{0\sigma}e^{-S_0}\langle exp[-\Delta S]\rangle^{(0)} \\ &= Z^{(0)}\int Dc^*_{0\sigma}Dc_{0\sigma}e^{-S_0}\langle exp[-\int_0^\beta d\tau\Delta S(\tau)\rangle^{(0)} \end{aligned} \tag{2.28}$$

with $\Delta S = \int_0^\beta d\tau\Delta S(\tau)$. Expanding eqn.(2.28) result in

$$\begin{aligned} Z &= Z^{(0)}\int Dc^*_{0\sigma}Dc_{0\sigma}e^{-S_0} \\ &\times \left(1-\int_0^\beta d\tau\langle\Delta S(\tau)\rangle^{(0)} + \frac{1}{2}\int_0^\beta d\tau_1\int_0^\beta d\tau_2\langle T_\tau\Delta S(\tau_1)\Delta S(\tau_2)\rangle^{(0)} + ...\right) \end{aligned} \tag{2.29}$$

where T_τ is the imaginary time ordering. In the case of fermions, which are considered here, the odd terms of the expansion vanishes, which however is not true for boson [32, 33]. So one can easily see that the lowest contribution is from the second term, which reads:

$$\begin{aligned} &\frac{1}{2!}\int_0^\beta d\tau_1\int_0^\beta d\tau_2\langle T_\tau\Delta S(\tau_1)\Delta S(\tau_2)\rangle^{(0)} \\ &= \frac{1}{2!}\int_0^\beta d\tau_1\int_0^\beta d\tau_2\langle T_\tau\sum_{i\sigma}[t_{i0}c^*_{i\sigma}(\tau_1)c_{0\sigma}(\tau_1)+t_{0i}c^*_{0\sigma}(\tau_1)c_{i\sigma}(\tau_1)] \\ &\times \sum_{j\sigma}\left[t_{j0}c^*_{j\sigma}(\tau_2)c_{0\sigma}(\tau_2)+t_{0j}c^*_{0\sigma}(\tau_2)c_{j\sigma}(\tau_2)\right]\rangle^{(0)} \\ &= \frac{1}{2!}\int_0^\beta d\tau_1\int_0^\beta d\tau_2\langle\sum_{ij\sigma}T_\tau\left[t_{i0}t_{0j}c^*_{i\sigma}(\tau_1)c_{0\sigma}(\tau_1)c^*_{0\sigma}(\tau_2)c_{j\sigma}(\tau_2)\right]\rangle^{(0)} \\ &+ \frac{1}{2!}\int_0^\beta d\tau_1\int_0^\beta d\tau_2\langle\sum_{ij\sigma}T_\tau\left[t_{0i}t_{j0}c^*_{0\sigma}(\tau_1)c_{i\sigma}(\tau_1)c^*_{j\sigma}(\tau_2)c_{0\sigma}(\tau_2)\right]\rangle^{(0)}. \end{aligned} \tag{2.30}$$

Now, we will show that the two parts in the eqn.(2.30) are equal. As for the first part one can take $\tau_1 < \tau_2$, which becomes

$$\begin{aligned}
&\frac{1}{2!}\int_0^\beta d\tau_1 \int_0^\beta d\tau_2 \langle \sum_{ij\sigma} T_\tau \left[t_{i0} t_{0j} c^*_{i\sigma}(\tau_1) c_{0\sigma}(\tau_1) c^*_{0\sigma}(\tau_2) c_{j\sigma}(\tau_2) \right] \rangle^{(0)} \\
&= \frac{1}{2!}\int_0^\beta d\tau_2 \int_0^\beta d\tau_1 \sum_\sigma c^*_{0\sigma}(\tau_2) \sum_{ij} t_{i0} t_{0j} \langle c_{j\sigma}(\tau_2) c^*_{i\sigma}(\tau_1) \rangle^{(0)} c_{0\sigma}(\tau_1). \qquad (2.31)
\end{aligned}$$

Because τ_1 and τ_2 are only dummy arguments, we can exchange them freely, which results in

$$\frac{1}{2!}\int_0^\beta d\tau_1 \int_0^\beta d\tau_2 \sum_\sigma c^*_{0\sigma}(\tau_1) \sum_{ij} t_{i0} t_{0j} \langle c_{j\sigma}(\tau_1) c^*_{i\sigma}(\tau_2) \rangle^{(0)} c_{0\sigma}(\tau_2). \qquad (2.32)$$

At the same time, the condition of $\tau_1 > \tau_2$, the second part in the bracket becomes

$$\frac{1}{2!}\int_0^\beta d\tau_1 \int_0^\beta d\tau_2 \sum_\sigma c^*_{0\sigma}(\tau_1) \sum_{ij} t_{0i} t_{j0} \langle c_{j\sigma}(\tau_1) c^*_{i\sigma}(\tau_2) \rangle^{(0)} c_{0\sigma}(\tau_2). \qquad (2.33)$$

As for the hopping amplitude, we always take the amplitude of the hopping into and out of the cavity site to be equal, $t_{0i} = t_{i0}$, it is same for 'j'. So one finds that Eqn.(2.32) and Eqn.(2.33) are same. So

$$\begin{aligned}
&\frac{1}{2!}\int_0^\beta d\tau_1 \int_0^\beta d\tau_2 \langle T_\tau \Delta S(\tau_1) \Delta S(\tau_2) \rangle^{(0)} \\
&= \int_0^\beta d\tau_1 \int_0^\beta d\tau_2 \sum_\sigma c^*_{0\sigma}(\tau_1) \sum_{ij} t_{i0} t_{0j} \langle T_\tau c_{i\sigma}(\tau_1) c^*_{j\sigma}(\tau_2) \rangle^{(0)} c_{0\sigma}(\tau_2) \\
&= -\int_0^\beta d\tau_1 \int_0^\beta d\tau_2 \sum_\sigma c^*_{0\sigma}(\tau_1) \sum_{ij} t_{i0} t_{0j} G^0_{ij}(\tau_1 - \tau_2) c_{0\sigma}(\tau_2) \qquad (2.34)
\end{aligned}$$

in which the cavity Green function $G^0_{ij}(\tau_1 - \tau_2)$ is identified. Similarly, all the higher order terms can be written in a similar way. The partition function can be written as:

$$\begin{aligned} Z &= Z^0 \int Dc^*_{0\sigma} Dc_{0\sigma} e^{-S_0} \\ &\times \left(1 - \int_0^\beta d\tau_1 \int_0^\beta \tau_2 \sum_\sigma c_{0\sigma}(\tau_1) \sum_{ij} t_{i0} t_{0j} G^0_{ij}(\tau_1 - \tau_2) c_{0\sigma}(\tau_2) + ...\right) \\ &= Z^0 \int Dc^*_{0\sigma} Dc_{0\sigma} e^{-S_0} exp[- \sum_{n=1}^{\infty} \sum_{i_1...i_n} \sum_{j_1...j_n} \int_0^\beta d\tau_{i_1}...d\tau_{i_n} d\tau_{j_n}...d\tau_{j_n} t_{i_1 0}...t_{i_n 0} \\ &\times t_{0j_1}...t_{0j_n} c^*_{0\sigma}(\tau_{i_1})...c^*_{0\sigma}(\tau_{j_n}) G^0_{i_1...i_n j_1...j_n}(\tau_{i_1}...\tau_{i_n}, \tau_{j_1}...\tau_{j_n}) c_{0\sigma}(\tau_{j_1})...c_{0\sigma}(\tau_{j_n})] \end{aligned} \tag{2.35}$$

where the $G^0_{i_1...i_n j_1...j_n}(\tau_{i_1}...\tau_{i_n}, \tau_{j_1}...\tau_{j_n})$ are 2n-point Green's functions of the lattice with the site 0 is removed. Returning back to the definition of the effective action Eqn. (2.25) we find

$$\begin{aligned} S_{eff} &= constant + S_0 + \sum_{n=1}^{\infty} \sum_{i_1...i_n} \sum_{j_1...j_n} \int_0^\beta d\tau_{i_1}...d\tau_{i_n} d\tau_{j_n}...d\tau_{j_n} t_{i_1 0}...t_{i_n 0} t_{0j_1}...t_{0j_n} \\ &\times c^*_{0\sigma}(\tau_{i_1})...c^*_{0\sigma}(\tau_{j_n}) G^0_{i_1...i_n j_1...j_n}(\tau_{i_1}...\tau_{i_n}, \tau_{j_1}...\tau_{j_n}) c_{0\sigma}(\tau_{j_1})...c_{0\sigma}(\tau_{j_n}). \end{aligned} \tag{2.36}$$

So we have obtained a single-site formulation of the problem, where the dynamics is described by the above effective action.

We can now use the simplification generated by the d$\longrightarrow \infty$ limit. As we have seen earlier, the t_{ij} scale like $d^{-\frac{1}{2}\|\mathbf{R}_i - \mathbf{R}_j\|}$, and so does the two-point Green's function $G^{(0)}_{ij}$. Therefore, the contribution for n=1 in Eqn. (2.36) is the order of one. When one consider the contribution for n $\geq$ 2, it turns out that they bring in a contribution of the order of at least $\frac{1}{d}$. Hence in the limit $d \longrightarrow \infty$ all contributions from n > 1

vanish and we are left with the following expression for S_{eff}

$$\begin{aligned} S_{eff} &= S_0 + \int_0^\beta d\tau_1 d\tau_2 \sum_\sigma c^*_{0\sigma}(\tau_1) \sum_{ij} t_{i0} t_{0j} G^{(0)}_{ij}(\tau_1 - \tau_2) c_{0\sigma}(\tau_2) \\ &= \int_0^\beta d\tau_1 d\tau_2 \sum_\sigma c^*_{0\sigma}(\tau_1) \mathcal{G}_0^{-1}(\tau_1 - \tau_2) c_{0\sigma}(\tau_2) + U \int_0^\beta d\tau n_{0\uparrow}(\tau) n_{0\downarrow}(\tau), \quad (2.37) \end{aligned}$$

where $\mathcal{G}_0$ denote the so called Weiss Green function and given by

$$\mathcal{G}_0^{-1}(\tau_1 - \tau_2) = -\left(\frac{\partial}{\partial \tau_1} - \mu\right) \delta\tau_1\tau_2 - \sum_{ij} t_{i0} t_{0j} G^{(0)}_{ij}(\tau_1 - \tau_2). \quad (2.38)$$

Fourier transforming to Matsubara frequency yields

$$\mathcal{G}_0^{-1}(i\omega) = i\omega + \mu - \sum_{ij} t_{i0} t_{0j} G^{(0)}_{ij}(i\omega). \quad (2.39)$$

Expression (2.39) is important because it relates the Weiss Green's function $\mathcal{G}_0$ to the Green's function $G^{(0)}_{ij}$ of the Hubbard model with one site is removed. In order to obtain a closed set of equation, one still needs to relate the latter to the Green's function of the original lattice. In the limit $d \to \infty$, relating Green's function to the lattice Green's function is easily performed by means of the following equation:

$$G^0_{ij} = G_{ij} - \frac{G_{i0} G_{0j}}{G_{00}},$$

which was derived already by Hubbard. Inserting this into eq. (2.39) gives

$$\mathcal{G}_0^{-1} = i\omega + \mu - \sum_{ij} t_{i0} t_{0j} G_{ij}(i\omega) - \frac{\left(\sum_i t_{i0} G_{i0}(i\omega_n)\right)^2}{G_{00}} \quad (2.40)$$

Further simplifications are achieved by inserting the **k**-space representation:

$$G_{ij}(i\omega_n) = \sum_{\mathbf{k}} e^{i\mathbf{k}.(\mathbf{R}_i - \mathbf{R}_j)} G_{\mathbf{k}}(i\omega_n),$$

where, by the expression of the tight-binding dispersion, it follows that

$$\sum_i t_{i0} G_{i0}(i\omega_n) = \sum_{\mathbf{k}} \sum_i t_{i0} e^{i\mathbf{k}.(\mathbf{R}_i - \mathbf{R}_0)} G_{\mathbf{k}}(i\omega_n) = \sum_{\mathbf{k}} \epsilon_{\mathbf{k}} G_{\mathbf{k}}(i\omega_n) \tag{2.41}$$

and

$$\sum_{ij} t_{i0} t_{0j} G_{ij}(i\omega_n) = \sum_{\mathbf{k}} \sum_{ij} t_{i0} t_{0j} e^{i\mathbf{k}.(\mathbf{R}_i - \mathbf{R}_0)} e^{i\mathbf{k}.(\mathbf{R}_0 - \mathbf{R}_j)} G_{\mathbf{k}}(i\omega_n) = \sum_{\mathbf{k}} \epsilon_{\mathbf{k}}^2 G_{\mathbf{k}}(i\omega_n). \tag{2.42}$$

Using equation (2.21)

$$G_{\mathbf{k}} = \frac{1}{\eta - \epsilon_{\mathbf{k}}}, \qquad \eta = i\omega_n + \mu - \Sigma(i\omega_n)$$

it is then straightforward to check the following identities

$$\sum_{\mathbf{k}} \epsilon_{\mathbf{k}} G_{\mathbf{k}} = \sum_{\mathbf{k}} \frac{\epsilon_{\mathbf{k}} - \eta + \eta}{\eta - \epsilon_{\mathbf{k}}} = -1 + \eta \sum_{\mathbf{k}} G_{\mathbf{k}} = -1 + \eta G_{00} \tag{2.43}$$

$$\sum_{\mathbf{k}} \epsilon_{\mathbf{k}}^2 G_{\mathbf{k}} = \sum_{\mathbf{k}} \frac{\epsilon_{\mathbf{k}}(\epsilon_{\mathbf{k}} - \eta) + \epsilon_{\mathbf{k}}\eta}{\eta - \epsilon_{\mathbf{k}}} = \eta \sum_{\mathbf{k}} \frac{\epsilon_{\mathbf{k}}}{\eta - \epsilon_{\mathbf{k}}} = -\eta + \eta^2 G_{00} \tag{2.44}$$

In views of equations $(2.41 - 2.44)$ equation (2.40) becomes:

$$\mathcal{G}_0^{-1}(i\omega_n) = \Sigma(i\omega_n) + G_{00}^{-1}(i\omega_n).$$

By using the short hand notation $G_{00} = G$ we arrive at the Dyson equation

$$\mathcal{G}_0^{-1}(i\omega_n) = \Sigma(i\omega_n) + G^{-1}(i\omega_n). \tag{2.45}$$

Bethe Lattice

The term Bethe lattice (*i.e.*, the Cayley tree with infinitely many lattice sites) refers to a pseudo-lattice, which lacks the possibility of closed paths (Fig. 2.2). This geometry

has attracted substantial interest because it offers both mathematical simplicity as well as densities of states with finite bandwidth.

On the Bethe lattice the summation of eqn.(2.39) can be restricted to $i = j$ (since neighbors of 0 are completely disconnected on this lattice once the cavity has been introduced), and again, in the limit of infinite connectivity, removing one site does not change the Green's function so that $G_{ij}^{(0)} = G_{ij}$ [11]. Using translational invariance, one finally obtain Eqn. (2.39) for the Weiss Green's function on the Bethe lattice:

$$\mathcal{G}_0^{-1}(i\omega) = i\omega + \mu - t^2 G(i\omega). \tag{2.46}$$

The half bandwidth is given by $D = 2t$ and we will use $D = 1$ as a unit of energy.

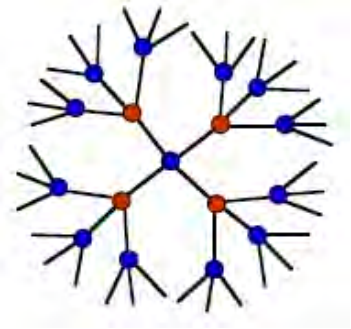

Fig. 2.2 Graph of a Bethe lattice with coordination factor z = 4 nearest neighbors.

In Hubbard model coupled to retarded interaction, the local charge degree of freedom is coupled to boson. As a result, the effective single-site problem can be thought of as an impurity coupled not only to a self-consistent fermionic bath but also to a self-consistent bosonic bath. Therefore, following the procedures as in section (2.4.3), and after integrating out the bosonic degree of freedom leads to a retarded interaction among the impurity electrons and is expressed as a contribution [34, 35]

$$S_{ret} = \frac{1}{2}\int_0^\beta d\tau \int_0^\beta d\tau' n(\tau) U_{ret}(\tau - \tau') n(\tau') \tag{2.47}$$

to effective action.

The retarded interaction in terms of $U_{ret}(\tau)$ and $U_{ret}(i\omega)$ respectively

$$U_{ret}(\tau) = \int_0^\infty \frac{d\omega'}{\pi} ImU_{ret}(\omega')B(\omega',\tau), \tag{2.48}$$

$$U_{ret}(i\omega_n) = -\int_0^\infty \frac{d\omega'}{\pi} ImU_{ret}(\omega')\frac{2\omega'}{(i\omega_n)^2 - \omega'^2}, \tag{2.49}$$

with $-\frac{1}{\pi}ImU_{ret}(\omega') = \lambda^2\delta(\omega' - \omega_0)$, and $B(\omega',\tau) = \frac{cosh[(\tau-\beta/2)\omega']}{sinh[\omega'\beta/2]}$ for $0 \leq \tau \leq \beta$ and periodically extended to $\tau + n\beta$ (n integer). In terms of the bosonic frequencies and coupling constants, the retarded interaction in (2.49) is explicitly given by

$$U_{ret}(i\omega_n) = -\frac{2\lambda^2\omega_0}{\omega_0^2 - (i\omega_n)^2} \tag{2.50}$$

and the full frequency-dependent interaction of the model reads

$$U(i\omega_n) = U + U_{ret}(i\omega_n). \tag{2.51}$$

In the infinite frequency limit, or for large frequencies compared to a characteristic frequency ω_0 in case of a single dominant bosonic mode, the interaction $U(i\omega_n)$ approaches the bare interaction: $U(i\omega_n \longrightarrow \infty) = U + U_{ret}(i\omega_n \longrightarrow \infty) = U$. This expresses the fact that screening becomes less effective at high energies. On the other hand, in the static limit and for small frequencies compared to the characteristic frequency, the interaction is given by

$$U_{eff} \equiv U + U_{ret}(i\omega = 0) = U - \frac{2\lambda^2}{\omega_0} < U. \tag{2.52}$$

2.5 Mapping onto an impurity model

Georges and Kotliar [29] pointed out that the effective single-site action (Eq 2.37) can be thought of as an impurity site coupled to a bath of conduction electrons and can be

parametrized by a single-impurity Anderson model (SIAM) [36]:

$$H_{AIM} = \sum_{p,\sigma} \epsilon_p a^\dagger_{p,\sigma} a_{p,\sigma} + \sum_{p,\sigma} [V_p d^\dagger_\sigma a_{p,\sigma} V^*_p a^\dagger_{p,\sigma} d_\sigma] + U n_\uparrow n_\downarrow - \mu(n_\uparrow - n_\downarrow). \tag{2.53}$$

Here p is the quantum number of the non interacting bath of electrons with creation operator $a^\dagger_{p,\sigma}$, $d^\dagger_\sigma(d_\sigma)$ are creation (annihilation) of impurity operators and V_p the hybridization describing the transition strength from impurity to the bath and vice versa. This Hamiltonian (eq. 2.53) is quadratic in $a^\dagger_{p\sigma}, a_{p\sigma}$: integrating out these give rise to an action of the form (2.37), with:

$$\mathcal{G}_0^{-1}(i\omega_n) = i\omega_n + \mu - \Delta(i\omega_n), \tag{2.54}$$

where $\Delta(i\omega_n)$ is the so-called hybridization function

$$\Delta(i\omega_n) = \sum_p \frac{|V_p|^2}{i\omega_n - \epsilon_p}. \tag{2.55}$$

The spectral representation eq. (2.55) is chosen as to reproduce the actual solution $\mathcal{G}$ of the mean field equation. The isolated site 0 plays the role of the impurity orbital, and the conduction bath is built out of all other sites. In other words, the effective single-site problem which the original Hubbard model is mapped onto can be seen as a particular SIAM. This mapping of the Hubbard model onto the single-impurity Anderson model results in dynamical mean field theory of self-consistent equations of the form:

$$G(i\omega_n) = G_{imp}(i\omega_n) \qquad and \qquad \Sigma(i\omega_n) = \Sigma_{imp}(i\omega_n) \tag{2.56}$$

For a Bethe lattice with infinite coordination number, the self-consistency conditions ($Eq.$2.56) can be reduced to a single equation, which simplifies the self-consistency cycle enormously and takes the form

$$\Delta(i\omega_n) = t^2 G(i\omega_n). \tag{2.57}$$

The DMFT self-consistency cycle: starting from an initial guess for $\mathcal{G}_0$ or Δ, the impurity Green's function $G(\tau) = -\langle T_\tau d(\tau) d^\dagger(\tau) \rangle$ is calculated using CT-HYB impurity solver. Fourier transforming this impurity Green's function ($G(i\omega_n)$) and inserting into eq. (2.46), one get new $\mathcal{G}_0$ for the next iteration. Far away from phase transitions this convergence is rather quick and is achieved within about 10 iterations. In the vicinity of phase transitions the convergence slows down considerably, but is usually achieved within at most 30 iterations.

Chapter 3

Continuous-Time Quantum Monte Carlo (CT-QMC)

The numerical renormalization group (NRG) methods extract low-energy description with in a small Hilbert space than the original problem using an iterative procedure [37], an idea which has been motivated by Wilson renormalization procedures [38]. It can operate directly on real frequencies. Similar to NRG, exact diagonalization (ED) works on real axis directly. ED has been widely applied to Quantum impurity models in the context of DMFT-simulations [39]. The bath is represented by a few bath sites due to the exponential scaling of the Hilbert space dimension. In contrast to the above impurity solver, the Hirsch-Fye QMC algorithm [12] and the continuous-time QMC algorithms [40] work directly with the effective action (2.37), in which the bath states have been integrated out, and thus do not need a truncation of the bath. However, they give direct access only to finite-temperature properties on the imaginary-time or imaginary-frequency axis. Real frequency data like spectra or optical conductivities have to be extracted via analytical continuation [41, 42].

For more than a decade, the Hirsch-Fye QMC algorithm was the only QMC impurity solver widely used in DMFT calculations. Since 2005, continuous-time QMC algorithms for impurity models [40] have been developed, which overcome some of

the limitations of the Hirsch-Fye algorithm, as they do not require a discretization of the imaginary time. The two most relevant solvers are the weak-coupling or interaction expansion continuous-time (CT-INT) algorithm [13] and the strong-coupling or hybridization-expansion continuous-time (CT-HYB) algorithm [14, 15]. The two solvers are complementary to each other, as they are based on an expansion in the interaction or the impurity-bath coupling, respectively. The CT-HYB algorithm has a more favorable theoretical scaling for increasing interaction and for decreasing temperature compared to the CT-INT algorithm [43], which makes it especially well suited for single site DMFT calculations for models with strong correlations but not too many orbitals. On the other hand, the CT-INT algorithm has, in general, a much more favorable theoretical scaling with system size, which makes it more suitable for cluster DMFT calculations or models with many orbitals as long as the interaction is not too strong.

The CT-HYB method has also been applied to variant of Kondo models [44, 45], where a localized spin interact with itinerant electrons via the exchange coupling. The method also applied to impurity models which include an additional bosonic field coupled to local degrees of freedom [34, 46]. The CT-HYB algorithm was first introduced for impurity models with impurity-bath couplings which are diagonal in the impurity degrees of freedom and which contain only density-density interactions [14]. This variant of the algorithm uses an efficient segment scheme for the description of the dynamics on the impurity, which is only applicable to models with density-density interactions. In this thesis, we use the segment picture of continuous-time hybridization expansion (CT-HYB) [1] version of the CT-QMC as the impurity solver and we review the basic ideas following Refs. [40, 49, 50].

[1] We used the code for CT-HYB impurity solver from the ALPS library [14, 47, 48]

3.1 Monte Carlo Basics

3.1.1 Definitions, Markov Chain and Metropolis Algorithm

In mechanics as well as quantum mechanics one is often faced with high dimensional sums or integrals over phase or configuration spaces which we denote generically by $\mathcal{C}$. To solve a thermodynamical system the quantity we have to calculate is the partition function Z [40].

$$Z = \int_{\mathcal{C}} dx p(x) \tag{3.1}$$

where $p(x)$ is the weight of one configuration/point in $\mathcal{C}$. In a classical system this is given by the Boltzmann weight $p(x) = exp(-\beta E(x))$ with $E(x)$ being the energy of the configuration x. For our approach the x is going to be a certain configuration in the space of all possible diagrammatic expansions of the partition function.

The expectation value of an observable O is given by the average over the configuration space $\mathcal{C}$ with the weight p normalized by the partition function Z:

$$\langle O \rangle = \frac{1}{Z} \int_{\mathcal{C}} dx O(x) p(x). \tag{3.2}$$

Here, the configuration x occurs with probability $\mathcal{P}(x) = \frac{p(x)}{Z}$ and the observable O takes the value $O(x)$ for configuration x. In general, the integration over the configurations in Eqn. (3.2) is complicated and a direct evaluation by integration over the whole configuration space is not feasible. If, however, many of the configurations have a very small probability $\mathcal{P}(x)$ and thus contribute very little to the expectation value (Eq. 3.2), it is not necessary to evaluate the whole integral over the configuration space and instead, a sequence of configurations $\{x_i\}$ can be created such that each configuration x is visited with a frequency according to its probability $\mathcal{P}(x)$. Then, the expectation value (Eq. 3.2) is given by

$$\langle O \rangle = \lim_{N \to \infty} \frac{1}{N} \sum_{i=1}^{N} O(x_i). \tag{3.3}$$

The sequence of configurations $\{x_i\}$ is called a Markov chain. The basic idea behind Monte Carlo sampling is to generate a Markov chain for the given probability distribution and use it to evaluate the desired expectation values.

To generate the Markov chain, a Markov process is used. In a Markov process the next move only depends on the current state the system is in with no memory of the past. It is fully characterized by a transition matrix W_{xy} specifying the probability to go from state x to state y in one step of the Markov process. Normalization requires $\sum_y W_{xy} = 1$ which guarantees that the probability stays normalized in the Markov process. Starting from an arbitrary distribution the Markov process will converge exponentially to a stationary distribution $p(x)$ if two conditions are satisfied

Ergodicity: Each configuration y has to be reachable from every configuration x with a finite number of Markov steps

Detailed balance: The probability distribution $p(x)$ and the transition matrix W_{xy} fulfill the equation

$$\frac{W_{xy}}{W_{yx}} = \frac{p_y}{p_x} \tag{3.4}$$

This condition is sufficient but not necessary – in principle we only need to fulfill the equilibrium condition $\sum_x p_x W_{xy} = p_y$

During the simulation, the first generated configurations are discarded to allow the Markov process to reach the equilibrium distribution, a step which is called thermalization. Then, the desired expectation values are approximated by averaging over a number of subsequently generated configurations.

The most widely used algorithm that fulfills the detailed balance condition is the Metropolis-Hastings algorithm [51, 52]. In this algorithm moves from the current configuration x to another configuration y are proposed with the probability W_{xy}^{prop} but only accepted with the probability W_{xy}^{acc}. If a move is rejected the old configuration is kept. The transition matrix is given by $W_{xy} = W_{xy}^{prop} W_{xy}^{acc}$. To satisfy the detailed balance condition we use

$$W_{xy}^{acc} = min[1, R_{xy}] \tag{3.5}$$

in the Metropolis algorithm, where R_{xy}, the acceptance ratio, is given by

$$R_{xy} = \frac{\mathcal{P}(y) W_{yx}^{prop}}{\mathcal{P}(x) W_{xy}^{prop}} \tag{3.6}$$

The acceptance ratio for the inverse move is simply given by $R_{yx} = R_{xy}^{-1}$. In an actual calculation we would draw a random number r $\in$ [0, 1] and accept the move if $R_{xy} < r$, otherwise reject it. To ensure ergodicity the moves which are proposed during the simulation have to be generated in such a way that we can reach any configuration possible. In CTQMC simulations these are the addition and removal of segments.

3.1.2 The Sign Problem

Until now we have tacitly assumed that the expansion coefficients of our partition function expansion are always positive or zero. This, and the fact that they stay finite, allows us to interpret the weights $p(x)/Z$ for configurations $x \in \mathcal{C}$ as a normalized probability density on the configuration space and allow the sampling with a Monte Carlo process. If the expansion coefficients $p(x)$ become negative, the p can no longer be regarded as a probability distribution on $\mathcal{C}$. This problem occurs when we are trying to solve fermionic problems in which the operators anti-commute. For these systems we have to find a strategy how to deal with the problem of changing signs in the probability.

The most often used approach is to sample the fermionic system with respect to the bosonic one by taking the absolute value of the weight $|p(x)|$ and to assign the sign $s(x) \equiv sgn\ p(x)$ to the observable which we are measuring

$$\langle O \rangle = \frac{\sum_x O(x) s(x) |p(x)| / \sum_x |p(x)|}{\sum_x s(x) |p(x)| / \sum_x |p(x)|} \tag{3.7}$$

The problem with the solution above is that if a sign problem occurs the error increases exponentially with the number of particles and the inverse temperature [53].

3.2 Partition Function Expansion

For the derivation of the partition function expansion which underline the CT-QMC algorithm, we consider the Anderson impurity model

$$H = H_{bath} + H_{loc} + H_{hyb} \tag{3.8}$$

with

$$\begin{aligned} H_{bath} &= \sum_{\sigma,p} \epsilon_p a^\dagger_{\sigma,p} a_{\sigma.p} \\ H_{loc} &= U n_\uparrow n_\downarrow - \mu \sum_\sigma n_\sigma \\ H_{hyb} &= \sum_{\sigma,p} V_p^\sigma d^\dagger_\sigma a_{\sigma,p} + \sum_{\sigma,p'} V_{p'}^{\sigma *} d_\sigma a^\dagger_{\sigma,p} = H_1^{d^\dagger} + H_1^d \end{aligned}$$

The partition function for the Anderson impurity model is given by

$$Z = Tr[e^{-\beta H}] \tag{3.9}$$

Decompose the Hamiltonian H into two parts $H = H_0 + H_1$ and rewrite the partition function in the interaction representation of H_0 and then expand in powers of H_1. We switch into the interaction representation by defining time-dependent operators $O(\tau)$ with respect to H_0 , *i.e.*,

$$O(\tau) = e^{\tau H_0} O e^{-\tau H_0}. \tag{3.10}$$

If we introduce the operator

$$A(\beta) = e^{\beta H_0} e^{-\beta H}, \tag{3.11}$$

the partition function Eqn. (3.9) can be written as

$$Z = Tr\left[e^{-\beta H_0} A(\beta)\right]. \tag{3.12}$$

The operator $A(\beta)$ has the property

$$\frac{dA(\beta)}{d\beta} = -H_1(\beta)A(\beta) \Longrightarrow A(\beta) = T_\tau exp\left[-\int_0^\beta d\tau H_1(\tau)\right]. \tag{3.13}$$

The partition function in the interaction representation follows as

$$Z = Tr\left[e^{-\beta H_0} T_\tau e^{-\int_0^\beta d\tau H_1(\tau)}\right]. \tag{3.14}$$

We can apply the time-ordering operator to the exponential and expand it in power of H_1:

$$Z = \sum_{n=0}^{\infty} \int_0^\beta d\tau_1 ... \int_{\tau_{n-1}}^\beta d\tau_n Tr\left[e^{(\beta-\tau_n)H_0}(-H_1)...e^{(\tau_2-\tau_1)H_0}(-H_1)e^{-\tau_1 H_0}\right], \tag{3.15}$$

which is sum of all configurations $\mathcal{C} = \{\tau_1, ..., \tau_n\}$, with n = 0, 1,..., and $\tau_n \in [0, \beta)$. In order to determine the optimal perturbation order n, we use Monte Carlo random walk to sample basically each order by the corresponding weight w_c

$$w_c = Tr\left[e^{(\beta-\tau_n)H_0}(-H_1)...e^{(\tau_2-\tau_1)H_0}(-H_1)e^{-\tau_1 H_0}\right] d\tau^n \tag{3.16}$$

There is the possibility to expand partition function Z (3.14) in H_{loc} or H_{hyb} which are known as the continuous-time interaction expansion (CT-INT) and continuous-time hybridization expansion(CT-HYB).

3.2.1 Continuous-time Hybridization Expansion (CT-HYB)

In the CT-HYB we choose $H_0 = H_{bath} + H_{loc}$ and $H_1 = H_{hyb}$. In view of these, Eqn. (3.14) becomes

$$Z = Tr\left[e^{-\beta(H_{loc}+H_{bath})} T_\tau e^{-\int_0^\beta d\tau H_{hyb}(\tau)}\right]. \tag{3.17}$$

Trace is taken over both the impurity and bath degrees of freedom. Here we expand the partition function over the hybridization term

$$Z = Tr\left[e^{-\beta H_0} T_\tau \sum_{n=0}^{\infty} \frac{(-1)^n}{n!}\left(-\int_0^\beta d\tau H_{hyb}(\tau)\right)^n\right] \tag{3.18}$$

The operator $H_{hyb} = H_1^{d^\dagger} + H_1^d$ has two terms: one that controls the hopping of electrons into the bath and one that contains the reverse process. As the operators $d_\sigma^\dagger$ and $a_{\sigma,p}$ occur only in $H_1^{d^\dagger}$, each such term has to be balanced by a H_1^d - term to yield a nonzero trace. Therefore only even powers of the expansion with alternating $H_1^{d^\dagger}$ and H_1^d contribute a nonzero trace: We can therefore write the partition function as a sum over configuration $c = \{\tau_1, ..., \tau_n; \tau_1', ..., \tau_n'\}$:

$$\begin{aligned} Z &= \sum_{n=0}^{\infty} \frac{1}{(n!)^2} \int_0^\beta d\tau_1 ... \int_{\tau_n}^\beta d\tau_n \int_0^\beta d\tau_1' ... \int_{\tau_n'}^\beta d\tau_n' \\ &\times Tr\left[e^{-\beta H_0} T_\tau H_1^d(\tau_n) H_1^{d^\dagger}(\tau_n') ... H_1^d(\tau_1) H_1^{d^\dagger}(\tau_1')\right]. \end{aligned} \tag{3.19}$$

Furthermore, using the time-ordering, the integrations for the two types of operators $H_1^{d^\dagger}$ H_1^dcan be ordered in time:

$$\begin{aligned} Z &= \sum_{n=0}^{\infty} \int_0^\beta d\tau_1 ... \int_{\tau_{n-1}}^\beta d\tau_n \int_0^\beta d\tau_1' ... \int_{\tau_{n-1}'}^\beta d\tau_n' \\ &\times Tr\left[e^{-\beta H_0} T_\tau H_1^d(\tau_n) H_1^{d^\dagger}(\tau_n') ... H_1^d(\tau_1) H_1^{d^\dagger}(\tau_1')\right]. \end{aligned} \tag{3.20}$$

Since the time evolution given by H_0 does not rotate the spin, there is an equal number of creation and annihilation operators for both spin up and down. Taking this into

account and writing out the expressions for H_1^d and $H_1^{d^\dagger}$ explicitly, we find

$$\begin{aligned} Z &= \sum_{\{n_\sigma\}} \prod_\sigma \int_0^\beta d\tau_1^\sigma ... \int_{\tau_{n\sigma-1}}^\beta d\tau_{n\sigma}^\sigma \int_0^\beta d\tau_1^{\prime\sigma} ... \int_{\tau_{n\sigma-1}^{\prime\sigma}}^\beta d\tau_{n\sigma}^{\prime\sigma} \\ &\times Tr[e^{-\beta H_0} T_\tau \prod_\sigma \sum_{p_1,...,p_{n\sigma}} \sum_{p_1',...,p_{n\sigma}'} V_{P_1}^\sigma V_{p_1}^{\prime\sigma *} ... V_{p_{n\sigma}}^\sigma V_{p_{n\sigma}}^{\prime\sigma *} \\ &\quad d_\sigma(\tau_{n\sigma}^\sigma) a_{\sigma,p_{n\sigma}'}^\dagger(\tau_{n\sigma}^\sigma) a_{\sigma,p_{n\sigma}'}(\tau_{n\sigma}^{\prime\sigma}) d_\sigma^\dagger(\tau_{n\sigma}^{\prime\sigma}) ... \\ &\quad d_\sigma(\tau_{1\sigma}^\sigma) a_{\sigma,p_{1\sigma}'}^\dagger(\tau_{1\sigma}^\sigma) a_{\sigma,p_{1\sigma}'}(\tau_{1\sigma}^{\prime\sigma}) d_\sigma^\dagger(\tau_{1\sigma}^{\prime\sigma})] \end{aligned} \tag{3.21}$$

Now, because the impurity and bath operate act on different spaces and H_0 does not mix the impurity and bath states, we can separate the trace over bath states and impurity states and write

$$\begin{aligned} Z &= Z_{bath} \sum_{\{n_\sigma\}} \prod_\sigma \int_0^\beta d\tau_1^\sigma ... \int_{\tau_{n\sigma-1}}^\beta d\tau_{n\sigma}^\sigma \int_0^\beta d\tau_1^{\prime\sigma} ... \int_{\tau_{n\sigma-1}^{\prime\sigma}}^\beta d\tau_{n\sigma}^{\prime\sigma} \\ &\times Tr_d[e^{-\beta H_{loc}} T_\tau \prod_\sigma d_\sigma(\tau_{n\sigma}^\sigma) d_\sigma^\dagger(\tau_{n\sigma}^{\prime\sigma}) ... d_\sigma(\tau_{1\sigma}^\sigma) d_\sigma^\dagger(\tau_{1\sigma}^{\prime\sigma})] \\ &\times \frac{1}{Z_{bath}} Tr_a[e^{-\beta H_{bath}} T_\tau \prod_\sigma \sum_{p_1,...,p_{n\sigma}} \sum_{p_1',...,p_{n\sigma}'} V_{P_1}^\sigma V_{p_1}^{\prime\sigma *} ... V_{p_{n\sigma}}^\sigma V_{p_{n\sigma}}^{\prime\sigma *} \\ &\quad a_{\sigma,p_{n\sigma}}^\dagger(\tau_{n\sigma}^\sigma) a_{\sigma,p_{n\sigma}'}(\tau_{n\sigma}^{\prime\sigma}) ... a_{\sigma,p_{n\sigma}}^\dagger(\tau_{1\sigma}^\sigma) a_{\sigma,p_{n\sigma}'}(\tau_{1\sigma}^{\prime\sigma})] \end{aligned} \tag{3.22}$$

where $Z_{bath} = Tr_a[e^{-\beta H_{bath}}] = \prod_\sigma \prod_p (e^{-\epsilon_p \beta} + 1)$. Since the bath is non-interacting, there is a Wick theorem for the bath and $Tr_a[...]$ can be expressed as the determinant of some matrix, whose size is equal to the perturbation order. To find the elements of this matrix, it is useful to consider the lowest perturbation order, $n_\sigma = 1$, $n_{\bar\sigma} = 0$. In this case

$$\begin{aligned} &\sum_{p_1} \sum_{p_1'} V_{p_1}^\sigma V_{p_1'}^{\sigma *} \frac{1}{Z_{bath}} Tr_a \left[e^{-\beta H_{bath}} T_\tau a_{\sigma,p_1}^\dagger(\tau_1^\sigma) a_{\sigma,p_1'}(\tau_1^{\prime\sigma}) \right] \\ &= \sum_{p_1} \frac{|V_{p_1}^\sigma|^2}{e^{\epsilon_{p_1}\beta} + 1} \begin{cases} e^{-\epsilon_{p_1}(\beta - (\tau_1^\sigma - \tau_1^{\prime\sigma}))} & \tau_1^\sigma > \tau_1^{\prime\sigma} \\ -e^{-\epsilon_{p_1}(\tau_1^{\prime\sigma} - \tau_1^\sigma)} & \tau_1^\sigma < \tau_1^{\prime\sigma} \end{cases} = \Delta_\sigma(\tau_1^\sigma - \tau_1^{\prime\sigma}). \end{aligned} \tag{3.23}$$

Introducing the β-antiperiodic hybridization function

$$\Delta_\sigma(\tau) = \sum_p \frac{|V_p|^2}{e^{\epsilon_p \beta}+1} \begin{cases} e^{-\epsilon_p(\beta-\tau)} & \tau > 0 \\ -e^{-\epsilon_p(-\tau)} & \tau < 0 \end{cases} \tag{3.24}$$

with $\Delta_\sigma(\tau)$ is the Fourier Transform of $\Delta_\sigma(-i\omega_n)$, which is connected to the non-interacting Green's function of SAIM via $\Delta_\sigma(-i\omega_n) = i\omega_n + \mu - \mathcal{G}_{0\sigma}(i\omega_n)^{-1}$, the first order result becomes $\Delta_\sigma(\tau_1^\sigma - \tau_1^{'\sigma})$. For higher order, the trace over the bath states can be expressed as

$$\begin{aligned} &\frac{1}{Z_{bath}} Tr_a[e^{-\beta H_{bath}} T_\tau \prod_\sigma \sum_{p_1,...,p_{n\sigma}} \sum_{p'_1,...,p'_{n\sigma}} V^\sigma_{P_1} V^{\prime\sigma *}_{p_1} ... V^\sigma_{p_{n\sigma}} V^{\prime\sigma *}_{p_{n\sigma}} \\ &\quad a^\dagger_{\sigma,p_{n\sigma}}(\tau^\sigma_{n\sigma}) a_{\sigma,p'_{n\sigma}}(\tau^{\prime\sigma}_{n\sigma}) ... a^\dagger_{\sigma,p_{n\sigma}}(\tau^\sigma_{1\sigma}) a_{\sigma,p'_{n\sigma}}(\tau^{\prime\sigma}_{1\sigma})] = \prod_\sigma det M^{-1}_\sigma \end{aligned} \tag{3.25}$$

where $M^{-1}_\sigma(i,j)$ is a $n_\sigma \times n_\sigma$ matrix with elements

$$M^{-1}_\sigma(i,j) = \Delta_\sigma(\tau^\sigma_i - \tau^{\prime\sigma}_j) \tag{3.26}$$

The weight coming from the trace over the bath states can therefore be absorbed into such a determinant and the expansion can be formulated as

$$\begin{aligned} Z &= Z_{bath} \sum_{\{n_\sigma\}} \prod_\sigma \int_0^\beta d\tau^\sigma_1 ... \int_{\tau_{n\sigma-1}}^\beta d\tau^\sigma_{n\sigma} \int_0^\beta d\tau^{\prime\sigma}_1 ... \int_{\tau^{\prime\sigma}_{n\sigma-1}}^\beta d\tau^{\prime\sigma}_{n\sigma} \\ &\times Tr_d[e^{-\beta H_{loc}} T_\tau \prod_\sigma d_\sigma(\tau^\sigma_{n\sigma}) d^\dagger_\sigma(\tau^{\prime\sigma}_{n\sigma}) ... d_\sigma(\tau^\sigma_{1\sigma}) d^\dagger_\sigma(\tau^{\prime\sigma}_{1\sigma})] \\ &\times \prod_\sigma M^{-1}_\sigma(\tau^\sigma_1, ..., \tau^\sigma_{n\sigma}; \tau^{\prime\sigma}_1, ...\tau^{\prime\sigma}_{n\sigma}) \end{aligned} \tag{3.27}$$

In the hybridization expansion method, the configuration space consists of all sequences $c = \{\tau^\uparrow_1, .., \tau^\uparrow_{n\uparrow}; \tau^{\prime\uparrow}_1, ..., \tau^{\prime\uparrow}_{n\uparrow} | \tau^\downarrow_1, .., \tau^\downarrow_{n\downarrow}; \tau^{\prime\downarrow}_1, ..., \tau^{\prime\downarrow}_{n\downarrow}\}$ of $n_\uparrow$ creation and annihilation operators for spin up ($n_\uparrow = 0, 1, ...$), and $n_\downarrow$ creation and annihilation operators for spin down

$(n_\downarrow = 0, 1, ...)$. The weight of this configuration is

$$\begin{aligned} w_c &= Z_{bath} Tr_d [e^{-\beta H_{loc}} T_\tau \prod_\sigma d_\sigma(\tau^\sigma_{n\sigma}) d^\dagger_\sigma(\tau'^\sigma_{n\sigma}) ... d_\sigma(\tau^\sigma_{1\sigma}) d^\dagger_\sigma(\tau'^\sigma_{1\sigma})] \\ &\times \prod_\sigma M^{-1}_\sigma(\tau^\sigma_1, ..., \tau^\sigma_{n\sigma}; \tau'^\sigma_1, ...\tau'^\sigma_{n\sigma})(d\tau)^{2n_\sigma}. \end{aligned} \tag{3.28}$$

For this, we write the partition function as

$$Z = \sum_c w_{\mathcal{C}} \tag{3.29}$$

The trace factor represents the contribution of the impurity, which fluctuates between different quantum states, as electrons hop in and out. The determinants re-sum all the bath evolutions which are compatible with the given sequence of transitions

Because the local Hamiltonian does not allow transitions between the flavors, for each flavor σ, a creation operator must be followed in time by annihilation operator and vice versa in the trace. This gives the constraint

$$\tau'^\sigma_1 < \tau^\sigma_1 < ... < \tau'^\sigma_n < \tau^\sigma_n \qquad or \qquad \tau^\sigma_1 < \tau'^\sigma_1 < ... < \tau^\sigma_n < \tau'^\sigma_n \tag{3.30}$$

Thus, the configuration c can be described by specifying for each flavor σ a set of n_σ consecutive creation and annihilation operator pairs, on the interval $[0, \beta)$, called 'segment'. We call the interval $[0, \beta)$ time-line. Fig. 3.1 illustrates exemplary segment configurations on the time-line of a flavor σ. The segments can either have all smaller start than end times (see Fig.3.1a), which corresponds to left hand side of the condition (3.30), or the last segment can wind around β (see Fig. 3.1b), which corresponds to the right hand side of the condition (3.30).

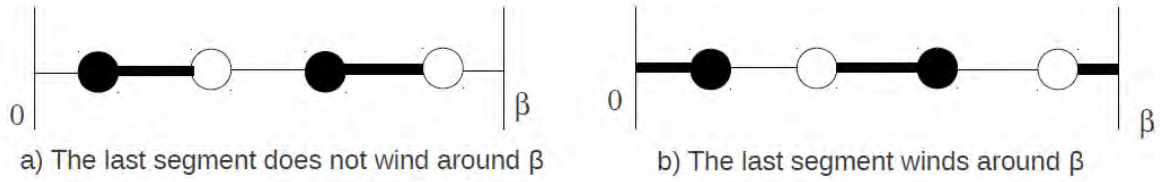

Fig. 3.1 Segment configurations on the time-line of a flavor σ at expansion order $n_\sigma = 2$ The start and end times of the segments, corresponding to creation and annihilation operators, are illustrated by closed circle and open circle, respectively.

Thus, in the segment picture, a configuration c is visualized by a collection of segments on the time-line from 0 to β for each flavor. The start of a segment (closed circles) is associated with an impurity creation operator, while an impurity annihilation operator is associated with the segment endpoint (open circles). A segment hence marks the imaginary time interval in which the impurity is occupied by an electron of a given flavor.

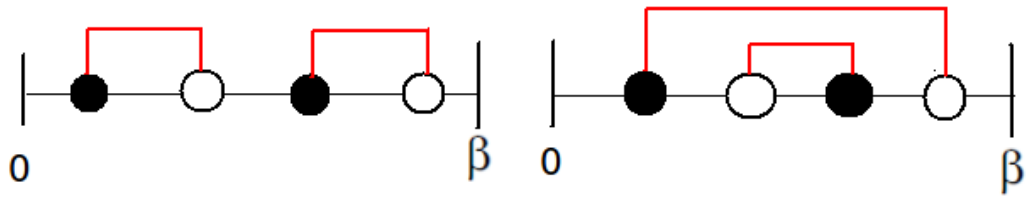

Fig. 3.2 Diagram for the illustration of the 2! ways of connecting hybridization line in a configuration with two segment for a given time line. Each end point τ_i^σ of a segment is connected to starting point $\tau_j'^\sigma$ by a red line representing $\Delta(\tau_j^\sigma - \tau_i'^\sigma)$. The combined weight of the diagrams can be expressed as a determinant (see Eqn.3.31).

The diagrams contributing to the partition function for $n_\sigma = 2$ of a given flavor are shown in Fig. 3.2. A diagram is depicted by a collection of segments. The collection of diagrams obtained by connecting the hybridization lines in all possible ways corresponds to the determinant:

$$det(\Delta) = \begin{vmatrix} \Delta(\tau_1^\sigma - \tau_1'^\sigma)\Delta(\tau_1^\sigma - \tau_2'^\sigma) \\ \Delta(\tau_2^\sigma - \tau_1'^\sigma)\Delta(\tau_2^\sigma - \tau_2'^\sigma) \end{vmatrix} \tag{3.31}$$

3.2.2 Density-density interaction

In this section we will see how to compute the contribution of trace over the impurity state:

$$w_{loc} = Tr_d[e^{-\beta H_{loc}} T_\tau \prod_\sigma d_\sigma(\tau^\sigma_{n\sigma}) d^\dagger_\sigma(\tau'^\sigma_{n\sigma}) ... d_\sigma(\tau^\sigma_{1\sigma}) d^\dagger_\sigma(\tau'^\sigma_{1\sigma})]. \tag{3.32}$$

If we restrict H_{loc} to density-density interactions (H_{loc} is diagonal in the occupation number basis) there exists a very efficient formulation of the hybridization algorithm, the so-called Segment implementation. To evaluate the trace factor for single orbital problem, we use the eigenbasis of H_{loc}:

$$H_{loc} = \begin{pmatrix} 0 & 0 & 0 & 0 \\ 0 & -\mu & 0 & 0 \\ 0 & 0 & -\mu & 0 \\ 0 & 0 & 0 & (U-2\mu) \end{pmatrix} \quad \text{in basis } |0\rangle, |\uparrow\rangle, |\downarrow\rangle, |\uparrow\downarrow\rangle. \tag{3.33}$$

In this basis, the time evolution operator is given by diag($e^{-\tau(0)}$, $e^{-\tau(-\mu)}$, $e^{-\tau(-\mu)}$, $e^{-\tau(U-2\mu)}$) while the operators d_σ and $d^\dagger_\sigma$ will produce transitions between eigenstates with amplitude ± 1.

Because the time evolution does not flip the spin, the creation and annihilation operators for given spin have to alternate. This allows us to separate the operators for spin up from those for spin down and to depict the time evolution by a collection of segments as in Fig. 3.3. The sum of all segment lengths is a measure of the average occupation on the impurity, which enters the local energy via the chemical potential term. Whenever two segments of opposite spin and/or orbital overlap it costs an additional energy $l_{overlap}$. The overall trace factor is (with s permutation sign)

$$W_{loc} = Tr_d[...] = sexp[\mu(l_\uparrow + l_\downarrow) - U l_{overlap}] \tag{3.34}$$

with l_σ the total length of the segments (*i.e.* the occupation) for spin σ and $l_{overlap}$ the total length of the overlap (*i.e.* the double occupation) between up and down segments.

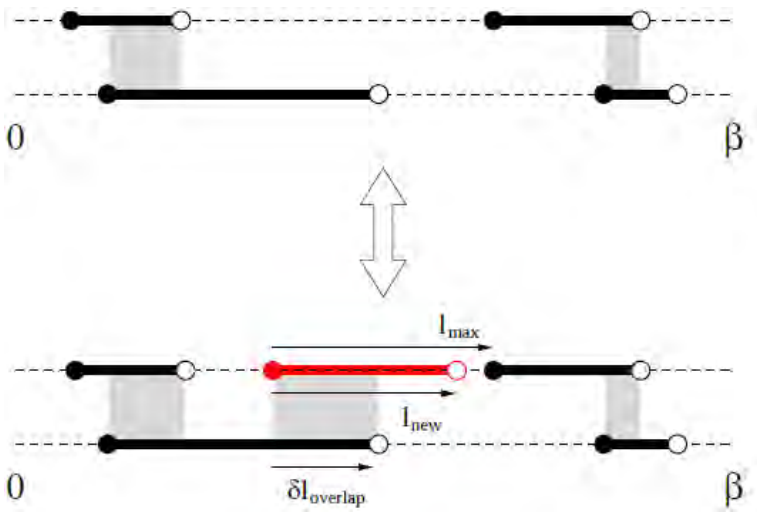

Fig. 3.3 Local update in the segment picture. The two segment configurations correspond to spin up and spin down. We increase the perturbation order by adding a segment or anti-segment of random length for random spin. The perturbation order is decreased by removing a randomly chosen segment [49].

3.2.3 Sampling procedure and detailed balance

The two basic updates required for ergodicity are the insertion and the removal of a segment. The diagrams of the partition function are sampled by randomly inserting or removing segments of varying length (and further moves to increase sampling efficiency). Empty and fully occupied states also have to be sampled.

We pick a random time in [0 to β) for the creation operator with probability $\frac{d\tau}{\beta}$. If it falls on an existing segment, the impurity is already occupied and the move is rejected. If it falls on an empty space, we compute l_{max}, the length from this position to the next segment (in the direction of increasing τ). If there are no segments, $l_{max} = \beta$. The position of the new annihilation operator is then chosen in this interval of length l_{max} with probability $\frac{d\tau}{l_{max}}$. The proposal probability to insert a segment is therefore:

$$W^{prop}(n_\sigma \longrightarrow n_\sigma + 1) = \frac{d\tau^2}{\beta l_{max}} \tag{3.35}$$

and the proposal probability to remove a segment is:

$$W^{prop}(n_\sigma + 1 \longrightarrow n_\sigma) = \frac{1}{n_\sigma + 1}. \tag{3.36}$$

The ratio of acceptance probabilities becomes

$$\begin{aligned} R(n_\sigma \longrightarrow n_\sigma + 1) &= \frac{W^{prop}(n_\sigma \longrightarrow n_\sigma + 1) w_{\mathcal{C}}(n_\sigma + 1)}{W^{prop}(n_\sigma + 1 \longrightarrow n_\sigma) w_{\mathcal{C}}(n_\sigma)} \\ &= \frac{\beta l_{max}}{n_\sigma + 1} e^{\mu l_{new} - U \delta l_{overlap}} \frac{|det(M_\sigma^{(n_\sigma+1)})^{-1}|}{|det(M_\sigma^{(n_\sigma)})^{-1}|} \end{aligned} \tag{3.37}$$

Therefore, the acceptance probability:

$$W^{acc} = min[1, R(n_\sigma \longrightarrow n_\sigma + 1)] \tag{3.38}$$

An important second update, equivalent to the insertion of a segment, is the insertion of an "anti segment": the insertion of a annihilator-creator pair instead of a creator-annihilator pair. The formulas for the acceptance ratio are the same as Eqn. (3.37). Besides smaller autocorrelation times these updates cause the two zero-order contributions "full occupation" and "no segment" to be treated on equal footing.

3.2.4 Measurement and Estimate of Observables

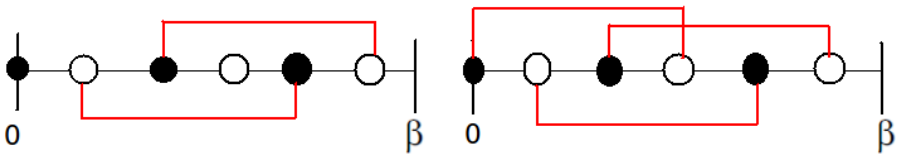

Fig. 3.4 Left: Diagram appearing in expansion of $G(\tau, 0)$. Right: Diagram with $d^\dagger$ at 0 and d at τ in expansion of Z.

For the measurements of the Green's function we want to make use of our partition function configurations. The idea is to remove hybridization lines from the configuration

to arrive at Green's function diagrams. In Fig. (3.4) we show two diagrams with the same operator sequence. On the left hand side a typical diagram in the expansion of $G(0,\tau) = -\langle T_\tau[d(\tau)d^\dagger(0)]\rangle$ of weight $W_c^{d(\tau),d^\dagger(0)}$ is shown, whereas on the right hand side we are dealing with a diagram in the expansion of Z with creation operator $d^\dagger$ at 0 and annihilation operator d at τ having a weight $W_c^{(\tau,0)}$. The Green's function can be written as

$$G(\tau,0) = \frac{1}{Z}\sum_c W_c^{d(\tau),d^\dagger(0)} = \frac{1}{Z}\sum_c W_c^{(\tau,0)}\frac{W_c^{d(\tau),d^\dagger(0)}}{W_c^{(\tau,0)}} \tag{3.39}$$

Since the trace factors of both weights are identical, and $\det M_c^{-1}$ is a minor of $\det(M_c^{(\tau,0)})^{-1}$, we find

$$\frac{W_c^{d(\tau),d^\dagger(0)}}{W_c^{(\tau,0)}} = \frac{detM_c^{-1}}{det(M_c^{(\tau,0)})^{-1}} = (M_c^{(\tau,0)})_{j,i} \tag{3.40}$$

with i and j denoting the row and column corresponding to the new operators $d^\dagger$ and d in the enlarged $(M_c^{(\tau,0)})^{-1}$. To transform the sum over c into a sum over configurations $\tilde{c} = \{c, \tau_i, \tau'_j\}$,the new operators must be free to be anywhere on the imaginary time interval, which (due to translational invariance) yields a factor $\frac{1}{\beta}\Delta(\tau, \tau_i - \tau'_j)$, with

$$\Delta(\tau.\tau') = \begin{cases} \delta(\tau - \tau') & \tau > 0 \\ -\delta(\tau - \tau' - \beta) & \tau' < 0 \end{cases} \tag{3.41}$$

Hence, the measurement formula for the Green's function becomes

$$G(\tau) = \frac{1}{Z}\sum_{\tilde{c}} W_{\tilde{c}} \sum_{i,j}\frac{1}{\beta}\Delta(\tau,\tau_i - \tau'_j)(M_{\tilde{c}})_{j,i} = \left\langle \sum_{i,j}\frac{1}{\beta}\Delta(\tau,\tau_i - \tau'_j)M_{j,i}\right\rangle_{MC} \tag{3.42}$$

In segment representation efficient estimators exist for the density, the double occupancy and the potential energy E_{pot}:

$$E_{pot} = UD, \qquad D_i = \langle n_{i\uparrow} n_{i\downarrow} \rangle_{MC} \tag{3.43}$$

The occupation n_σ is estimated by the length l_σ (3.34) of all the segments $n_\sigma = \langle \frac{l_\sigma}{\beta} \rangle$. A site is doubly occupied if the two orbitals overlap, and therefore $\langle D_i \rangle = \frac{1}{\beta} \langle l_{overlap} \rangle$. In the context of DMFT, the average expansion order $\langle k \rangle$ is related to the kinetic energy per site as

$$E_{kin} = -\frac{\langle k \rangle}{\beta} \tag{3.44}$$

3.3 Retarded Interaction in CT-HYB

In this section we present how to apply continuous-time hybridization expansion (CT-HYB) techniques to a problem which involve a coupling of impurity charge to bosons *i.e.*, we present how to treat the additional bosonic field in CT-HYB [40].

Previous treatment of retarded effect within exact diagonalization, numerical renormalization group requires truncation of bosonic Hilbert space, retaining only a finite number of boson states [54–57]. However, CT-HYB method, which has been exploited recently, can be applied to such problem without truncation of the boson Hilbert space. In this method, the electron-phonon coupling is eliminated by the so-called Lang-Firsov transformation, which leads to a modified Monte Carlo weight which contains an interaction between all pairs of hybridization events, and can be computed at essentially no additional computational cost [46].

The dynamical mean-field theory (DMFT), which is exact in infinite spatial dimensions [11], maps a lattice problem onto an effective impurity problem. The

effective impurity model for Hubbard-Holstein Hamiltonian (Eq.2.11) is given by

$$
\begin{aligned}
H_{eff} &= H_{loc} + H_{bath} + H_{hyb}, && (3.45)\\
H_{loc} &= -\mu(n_\uparrow + n_\downarrow) + U n_\uparrow n_\downarrow + \lambda(n_\sigma - 1)(b^\dagger + b) + \omega_0 b^\dagger b && (3.46)\\
H_{bath} &= \sum_{p,\sigma} \epsilon_p a^\dagger_{p,\sigma} a_{p,\sigma} && (3.47)\\
H_{hyb} &= \sum_{p,\sigma} V_p d^\dagger_\sigma a_{p,\sigma} - V_p^* d_\sigma a^\dagger_{p,\sigma} && (3.48)
\end{aligned}
$$

where $a_p(a_p^\dagger)$ is an annihilation (creation) operator of the electron in the effective bath with bath state labeled by quantum number p, $d_\sigma(d_\sigma^\dagger)$ is an annihilation (creation) operator of the electron on the impurity. The bath (H_{bath}) and the hybridization (H_{hyb}) terms are determined self-consistently in such a way that the impurity Green's function reproduces the local lattice Green's function of the Hubbard-Holstein model.

3.3.1 Canonical Transformation

By introducing the operator and corresponding conjugate momentum

$$\phi := \frac{1}{\sqrt{2}}(b^\dagger + b), \qquad \Pi := \frac{1}{i\sqrt{2}}(b^\dagger - b) \tag{3.49}$$

which obey $[\Pi, \phi] = i$, one can write an alternative representation for the local Hamiltonian (3.47) as

$$H_{loc} = -\mu(n_\uparrow + n_\downarrow) + U n_\uparrow n_\downarrow + \sqrt{2}\lambda(n_\sigma - 1)\omega_0(\phi^2 + \Pi^2). \tag{3.50}$$

Following refs.[40, 46], we can decouple $n_\sigma = n_\uparrow + n_\downarrow$ and boson by performing a canonical transformation $\tilde{H}_{loc} = e^S H_{loc} e^{-S}$ with $S = i\phi_0\Pi = \lambda/\omega_0(b^\dagger - b)(n_\sigma - 1)$, which shifts ϕ by $\phi_0 = \sqrt{2}\lambda/\omega_0(n_\sigma - 1)$. The transformed effective impurity model

Hamiltonian $\tilde{H}_{eff}$ is given by

$$\tilde{H}_{eff} = e^{S} H_{eff} e^{-S} = \tilde{H}_{loc} + H_{bath} + \tilde{H}_{hyb}, \tag{3.51}$$

$$\tilde{H}_{loc} = -\tilde{\mu}(n_{\uparrow} + n_{\downarrow}) + \tilde{U} n_{\uparrow} n_{\downarrow} + \frac{\omega_0}{2}(\phi^2 + \Pi^2), \tag{3.52}$$

$$\tilde{H}_{hyb} = \sum_{p,\sigma} V_p \tilde{d}^{\dagger}_{\sigma} a_{p,\sigma} - V_p^{*} \tilde{d}_{\sigma} a^{\dagger}_{p,\sigma} \tag{3.53}$$

which has no explicit electron-phonon coupling. $\tilde{H}_{loc}$ is of the Hubbard form but with modified chemical potential and interaction strength: $\tilde{\mu} = \mu - \lambda^2/\omega_0$, $\tilde{U} = U - 2\lambda^2/\omega_0$. The impurity electron creation and annihilation operators are transformed according to $\tilde{d}^{\dagger}_{\sigma} = e^{S} d^{\dagger}_{\sigma} e^{-S} = d^{\dagger}_{\sigma} e^{(\lambda/\omega_0)(b^{\dagger} - b)}$, and $\tilde{d}_{\sigma} = e^{S} d_{\sigma} e^{-S} = d_{\sigma} e^{-(\lambda/\omega_0)(b^{\dagger} - b)}$ respectively and this factor propagates in to the hybridization.

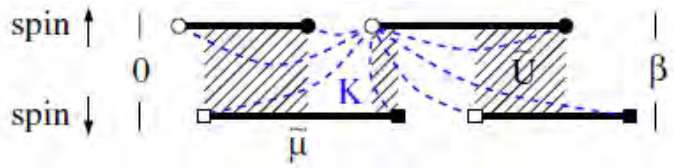

Fig. 3.5 (color online). Illustration of an order $n = 4$ diagram for one orbital Holstein-Hubbard model. Empty (full) circles and squares represent $V^{\dagger}(V)$ hybridization events. Dashed lines indicate interactions $K(\tau)$ connecting all pairs of hybridization events [40].

With the transformed effective impurity model, the total weight of a configuration is

$$w(\{\tau_i\}) = \tilde{w}_{loc}(\{\tau_i\}) w_{hyb}(\{\tau_i\}) w_b(\{\tau_i\}) \tag{3.54}$$

The first two are the configuration from the Anderson impurity model: the local weight $\tilde{w}_{loc}$ corresponds to configuration in the Hubbard impurity model (without phonon but modified parameters $\tilde{U}$ and $\tilde{\mu}$), and w_{hyb} denotes the trace over the fermionic operators, which is expressed by the determinant of hybridization function.

The third factor $w_b(\{\tau_i\})$ (weight due to retarded interaction) is a contribution of boson, which is the expectation of product of exponential of non interacting boson

operators and is given as

$$w_b(\{\tau_i\}) = \langle e^{s_{2n}A(\tau_{2n})}...e^{s_1A(\tau_1)}\rangle_b \tag{3.55}$$

with $0 \leq \tau_1 < \tau_2 < ... < \tau_{2n} < \beta$, s_i =1(-1) if the n^{th} operator is a creation (annihilation) operator and $A(\tau) = \lambda/\omega_0 \times (e^{\omega_0\tau}b^\dagger - e^{-\omega_0\tau}b)$. The thermal average can be evaluated analytically to give [34]

$$w_b(\{\tau_i\}) = exp\left[\sum_{2n\geq i\geq j\geq 1} s_i s_j K(\tau_i - \tau_j\right], \tag{3.56}$$

$$K(\tau) = -\frac{\lambda^2}{\omega^2}\frac{cosh[\omega_0(\tau - \beta/2)] - cosh[\omega_0\beta/2]}{sinh[\omega_0\beta/2]}. \tag{3.57}$$

As illustrated in Fig. 3.5, the retarded interaction contribution to the weight factor amounts to a nonlocal interaction between all pairs of hybridization events. Since the computational bottleneck is the handling of the hybridization matrix determinants, the additional weight factor w_b does not significantly slow down the simulation [46].

Chapter 4

Mott Transition in Hubbard Model on Bethe Lattice

4.1 Introduction

In strongly correlated systems, the correlation induced metal-insulator transition is one of the fundamental theoretical problems in condensed matter physics, and continues receive intensive attention [11]. It is realized experimentally in three dimension transition metal oxides, such as V_2O_3, and can be driven by application of pressure, temperature, and composition [9, 58]. The metallic state far from the transition is well described by the Fermi liquid theory, illustrating the wave-like properties of electrons in solids. In insulating side, the electrons behave as a localized particle. Near the transition, the effective Coulomb repulsion between carriers is the same order as the kinetic energy term. This regime probes the dual character of electron, namely, the particle and wavelike character, and requires a non-perturbative method for its description.

The nature of MIT of the half-filled one-band Hubbard model with only nearest neighbor hopping depends strongly on whether translational lattice symmetry break or not. If translational symmetry does not break, the only competing phases are

paramagnetic metal and paramagnetic insulator. The insulating state has an entropy of $\ln 2$ per site, which corresponds to the two degenerate spin direction for each localized spin in paramagnetic Mott insulator. The metallic state is a Fermi liquid with a heavy mass. The mass increases as the transition is approached to match the large entropy of the paramagnetic insulator. This is the essence of the Brinkman-Rice theory of MIT, which has been substantially extended by single-site DMFT of the Hubbard Model in the paramagnetic phases. The key prediction of this approach, such as the existence of a first order line ending in the second order point and numerous high temperatures crossover, have been verified experimentally [59].

However, in the case of a bipartite lattice (lattice translational symmetry break) and if t_{ij} is restricted to nearest neighbors (NNs) hopping, the Mott transition at half-filling quite generally does not occur, since it is acquired by the intrinsic weak-coupling instability toward anti-ferromagnetic (AF) long-range order. Anti-ferromagnetic order breaks the translational symmetry of the lattice causing a doubling of the unit cell. In momentum space, the doubling of unit cell results in a reduction of the first Brillouin zone. The resulting anti-ferromagnetic Brillouin zone possesses only half of the original volume.

In lines first drawn by Slater [60], the back-folding of the conduction band into the reduced Brillouin zone combined with the opening of a gap at the new zone boundary causes the ordered state to be an insulator. This insulating behavior is primarily induced by symmetry breaking

We here intend to see (examine) the finite temperature Mott-Hubbard transition in the single band Hubbard Model. Previous extensive studies help us to understand the qualitative nature of the Mott transition in the Hubbard Model. There exist a critical temperature above which only a smooth crossover occurs between a metal and a Mott insulator [11]. Below the critical temperature, however, a coexistence region separates the metallic phase from Mott insulating phase, which implies that the system undergoes a first-order phase transition somewhere inside the coexistence region [11].

4.2 Formalism

In this work we consider single band Hubbard model, the minimal model which describes strongly correlated electrons on a lattice, whose Hamiltonian is

$$H = \sum_{\langle i,j\rangle\sigma} t_{ij}[d^{\dagger}_{i\sigma}d_{j\sigma} + d_{i\sigma}d^{\dagger}_{j\sigma}] - \mu\sum_{i}[n_{i\uparrow} + n_{i\downarrow}] + U\sum_{i} n_{i\uparrow}n_{i\downarrow} \tag{4.1}$$

where i, j denotes sites, σ is the spin, and the first sum is over nearest neighbors. $d^{\dagger}_{i,\sigma}$ denotes a creation operator of an electron, t_{ij} is the hopping parameter, U is the on-site electron-electron interaction, μ is the chemical potential.

The non-interacting DOS $\rho_0(\epsilon)$ on the Bethe lattice becomes semi-circular in the limit of infinite dimension (infinite coordination number),

$$\rho_0(\epsilon) = \frac{2}{\pi D}\sqrt{1-(\epsilon/D)^2} \tag{4.2}$$

with a half bandwidth $D = 2t$ and we set $D = 1$ as a unit of energy. By using the semi-circular density in eq. (4.2), the self-consistency condition is

$$\Delta(\tau) = t^2 G(\tau). \tag{4.3}$$

We employ the single-site DMFT, which maps interacting lattice model onto local problem, called effective quantum impurity model, and a self-consistent condition. The impurity model is solved using the strong coupling version of the continuous time quantum Monte Carlo (CT-QMC) method - the continuous time hybridization expansion (CT-HYB) [14, 15, 40], which provides numerically exact solution of the impurity problem.

4.3 Results and Discussion

4.3.1 Quasi-particle and Spectral weights at the Fermi level

Self-energy Σ determines the physical properties of the quasi-particles. It leads to a change of the effective mass of the quasi-particle. Self-energy can be measured directly from the DMFT +CT-QMC simulation. Within DMFT, because self-energy is momentum independent, the effective mass of quasi-particle is directly related to Z: $\frac{m^*}{m} = \frac{1}{Z}$, where m^* is the quasiparticle effective mass and m is the bare electron mass. One can determine the quasi-particle weight Z from self-energy by [61]

$$Z = \frac{1}{1 - \frac{\partial Re\Sigma(\omega)}{\partial \omega}|_{\omega=0}}. \tag{4.4}$$

The physical meaning of Z is clear for the paramagnetic state at $T = 0$, where the system is either a Fermi liquid (for $U < U_c$) or an insulator (for $U > U_c$). The vanishing of Z therefore marks the metal-insulator transition at $T = 0$. However, for finite temperature QMC simulations, the derivative of the real part of self-energy component is approximated [62] (see Ref. [61] and Refs. within) by $Im\Sigma(i\omega_0)/\omega_0$, with $\omega_0 = \pi/\beta$, the first Matsubara frequency. So the quasi-particle weight for finite temperature is given as:

$$Z = \frac{1}{1 - \frac{Im\Sigma(i\omega)}{\omega_0}}. \tag{4.5}$$

Metallic and insulating states are defined based on the spectral function or density of state (DOS) at Fermi level. If DOS is different from zero, it is a metal, otherwise there exist an energy gap at the Fermi level and the system is an insulator. In DMFT + CT-QMC calculations, the phase boundary between metal and Mott insulator is idenfined directly by measuring the imaginary time Green's function. $\beta/\pi(G(\tau = \beta/2))$ can be viewed as a representation of integrated spectral weight [50, 62], and related to

density of states at the Fermi energy by

$$\frac{\beta}{\pi}G(\tau=\beta/2)=\frac{\beta}{\pi}\int d\omega\frac{A(\omega)}{2\cosh(\beta\omega/2)}\longrightarrow A(\omega=0)\qquad as\qquad T\longrightarrow 0. \tag{4.6}$$

If the temperature is low enough, then the value of $\beta/\pi(G(\tau=\beta/2))$ gives a good estimate of the value of the spectral function $A(\omega=0)$.

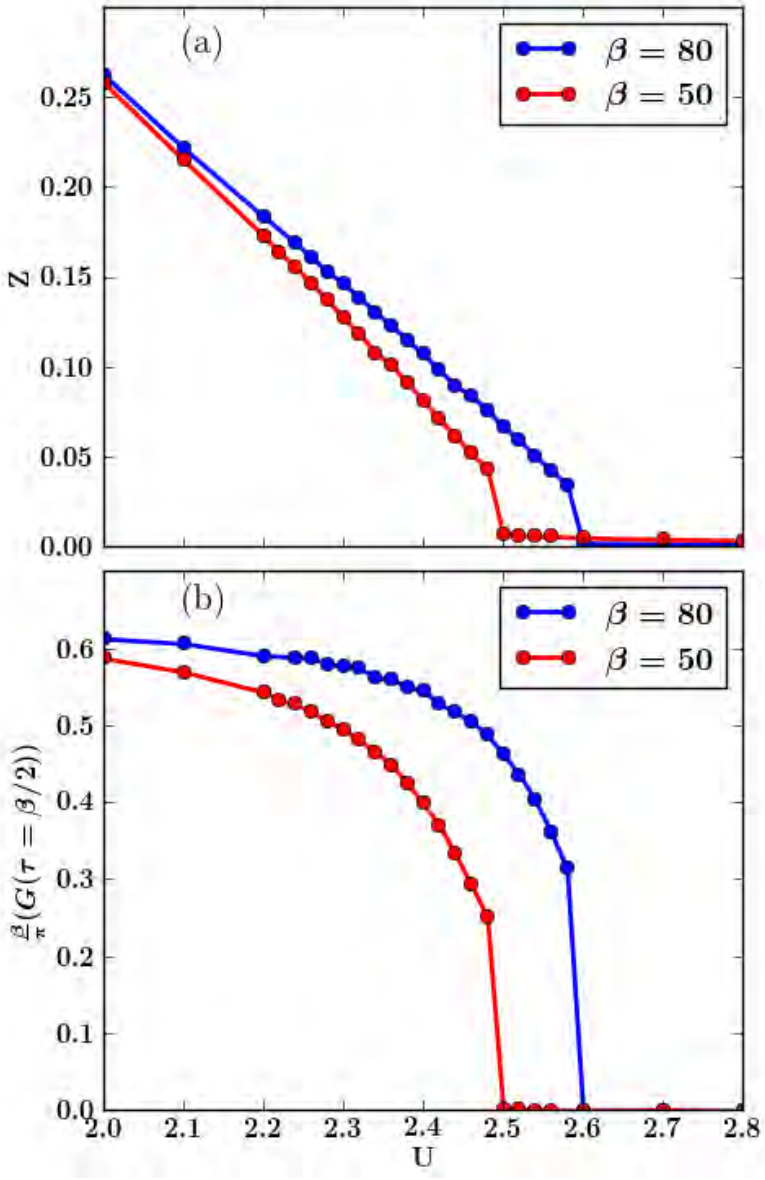

Fig. 4.1 Quasiparticle weight Z (a), and DOS (b) versus interaction U at temperatures $T=1/50$ [red circle] and $T=1/80$ [blue circle].

The phase boundary between metal and Mott insulator is signaled by a vanishing quasiparticle weight Z at the Fermi level (at T=0). We increased the on-site interaction U step by step to approach the phase transition. Figure 4.1 (a) shows the quasiparticle weight Z as a function of interaction U for temperatures, $T = 1/50$ and $T = 1/80$. The calculated quasiparticle weight Z is a good approximation for our low temperatures and indicate the Mott insulator transition are at $U_{c2} \approx 2.50$ and $U_{c2} \approx 2.60$ for temperature $T = 1/50$ and $T = 1/80$ respectively. The driving force behind the Mott transition is the blocking of charge degrees of freedom.

In Fig. 4.1 (b) we show $\beta/2(G(\tau = \beta/2))$ as a function of interaction U at temperatures $T = 1/50$ and $T = 1/80$. For $T = 1/50$ and $T = 1/80$, the values of $\beta/2(G(\tau = \beta/2))$ decreases and goes to approximately zero and the insulating gap at Fermi energy opens at on-site interactions $U_{c2} \approx 2.50$ and $U_{c2} \approx 2.60$ at temperatures $T = 1/50$ and $T = 1/80$ respectively. $\beta/\pi(G(\tau = \beta/2))$ increases as T decreases, indicating the development of a coherent Fermi-liquid state. The critical U is seen to be essentially temperature dependent indicating that the entropies of the metallic and non-metallic states are different.

4.3.2 Double Occupancy and Energy Density

Here we attempt to analyze the competition of the phases in terms of double occupancy and energy densities. These observables are measured directly from continuous-time hybridization expansion [50], and are expressed by equations (3.43) and (3.44).

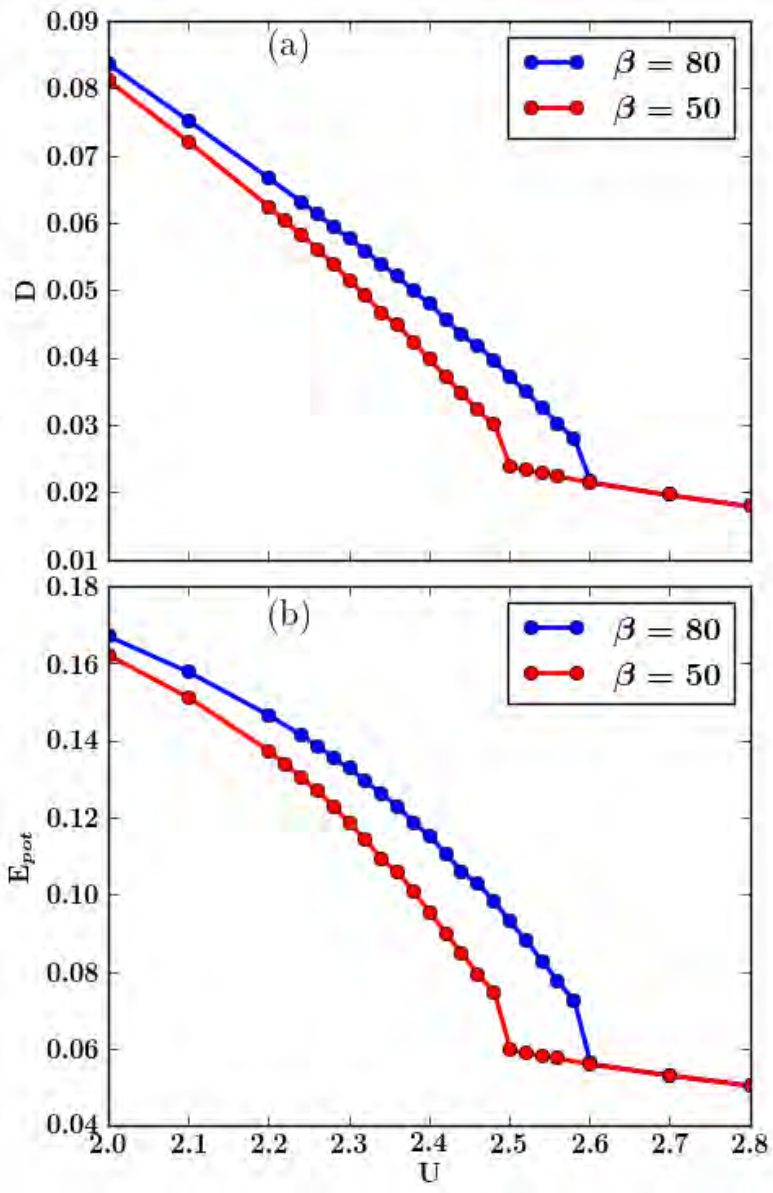

Fig. 4.2 (Color online) Double occupancy D (a), and (b) Potential energy E_{pot} versus interaction U at temperatures $T = 1/50$ [red circle] and $T = 1/80$ [blue circle].

In Fig. 4.2 (a) we show the results for double occupancy D as a function of on-site interaction U at temperatures $T = 1/50$ and $T = 1/80$. As the on-site interaction increases, the double occupancy smoothly decreases. The double occupancy increases in metallic phase ($U < U_c$) as the temperature T decreases, while it is almost independent of temperature T in the insulating phase ($U > U_c$). The increase of double occupancy

at low temperature means the suppression of the local moments due to the formation of quasiparticles.

The potential energy $E_{pot} = UD$ as a function of on-site interaction is shown in Fig. 4.2 (b) at temperature $T = 1/50$ and $T = 1/80$. Obviously, our interpretation on the double occupancy carry over to the potential energy.

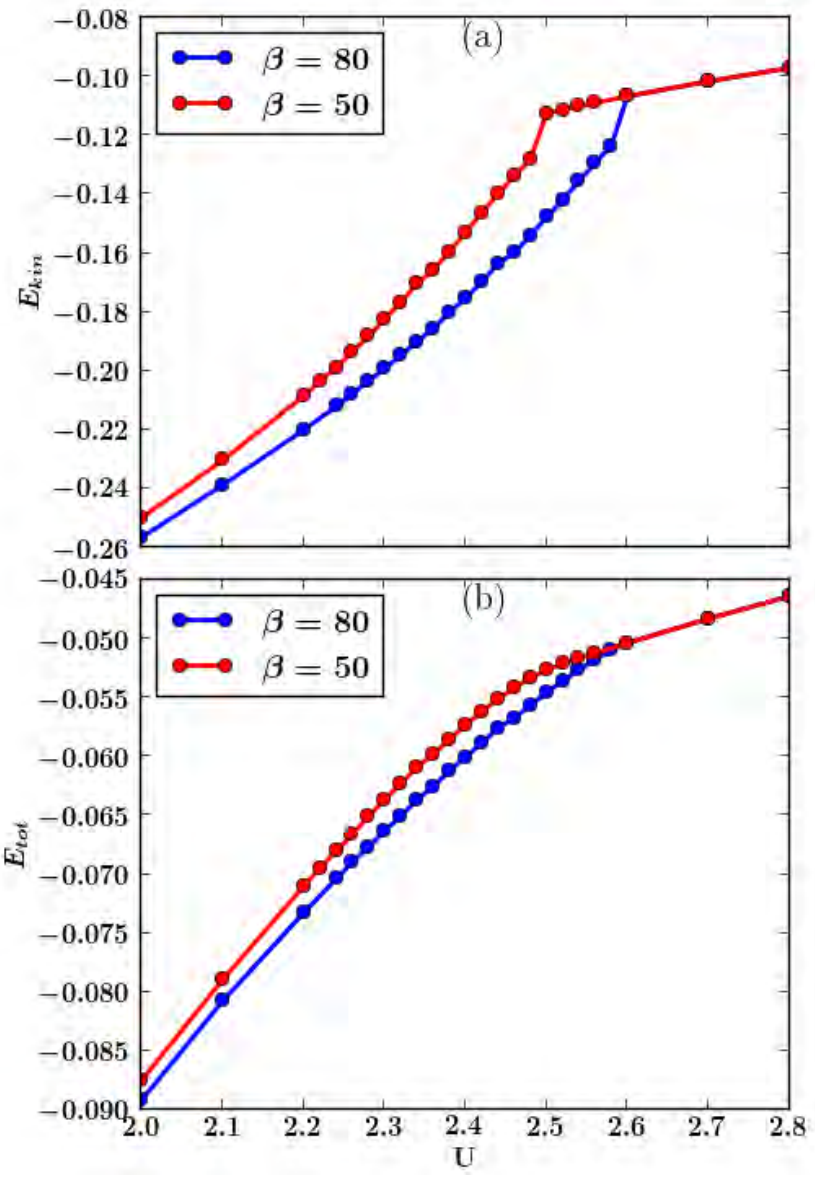

Fig. 4.3 (Color online) Kinetic energy E_{kin} (a), and Total energy E_{tot} versus interaction U at temperatures $T = 1/50$ [red circle] and $T = 1/80$ [blue circle].

The kinetic energy as a function of on-site interaction U for temperatures $T = 1/50$ and $T = 1/80$ is shown in Fig. 4.3 (a). The kinetic energy increases as the temperature decreases.

Fig. 4.3 (b) show total internal energy as a function of on-site interaction U for temperatures $T = 1/50$ and $T = 1/80$. The graph is linear on metallic side up to some transition point which decreases from approximately $U_{c2} \approx 2.50$ for $T = 1/50$ and $U_{c2} \approx 2.60$ for $T = 1/80$. On insulating side, the curve is linear but with decreasing slope. As can be seen from the figure, the total internal energy in the insulating phase is independent of temperature. Such universal behavior is expected deep inside the insulating low-temperature phase where a well-developed gap in the spectrum exists at the Fermi energy and where thermal excitations are suppressed exponentially [63].

As can be seen from Fig. 4.3 (b), the metal remains stable & closely follows the linear dependence of on-site interaction U until its energy almost reaches the insulating at U_{c2}, i.e., the metallic phase closely approaches the insulating phase in terms of energy which is consistent with the earlier report [63]. Such behavior is not generically expected for the first-order transition. However, recently A. J. Kin et al., reported that the total energy shows a discontinuous jump to a value of U_{c2}[64].

4.3.3 Linear Coefficient of Specific Heat

We estimate the linear coefficient of the specific heat γ from the density of states A at the Fermi energy and the quasi-particle weight Z, which are obtained from measured imaginary time Green's function via eqn. (4.6) and from the Matsubara self-energy via eqn.(4.5). Mathematically, we have [65]

$$\gamma = \frac{2\pi k_B^2}{3} \frac{A}{Z}. \tag{4.7}$$

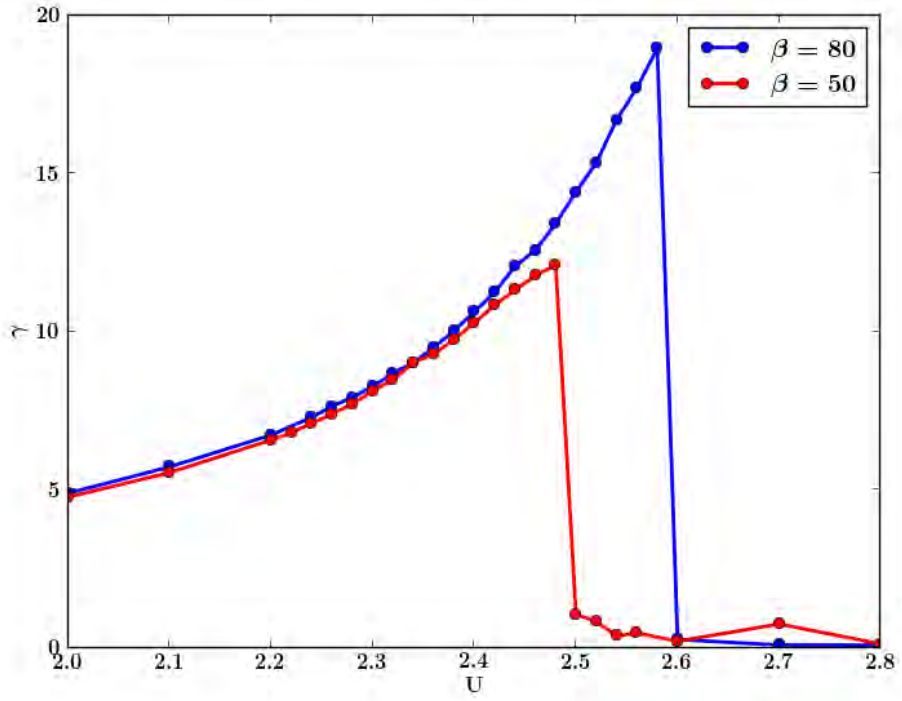

Fig. 4.4 Coefficient of heat capacity γ versus interaction U at temperature $T = 1/50$ [red circle] and $T = 1/80$ [blue circle].

Figure 4.4 shows the coefficient of specific heat as a function of interaction U for two values of temperatures, $T = 1/50$ and, $T = 1/80$. As seen in the figure the coefficient of specific heat initial increases as U increases, then abruptly drops at $U_{c2} \approx 2.50$ and $U_{c2} \approx 2.6$, which are indication of the critical points for Mott insulator, possibly because of the disappearance of quasiparticle, for $\beta = 50$ and $\beta = 80$, respectively. The increase in linear coefficient of specific heat (γ) as the on-site interaction U increase is due to the mass enhancement ($\gamma \propto m^*$) as the transition approached to match the large entropy of paramagnetic insulating state. Lowering temperature causes the drop in the coefficient of specific heat to occur at larger values of critical interaction U and an overall higher values for the coefficient of specific heat. As can be seen from Fig. 4.4, the coefficient of specific heat in the insulating phase seems to be roughly independent of temperature. The specific heat $C = \gamma T$ in insulating state is much smaller than the metallic state.

4.4 Conclusion

We have studied correlation-driven metal-insulator transition in a single band Hubbard model on Bethe lattice using single-site dynamical mean-field theory, which is exact in infinite spatial dimension, with continuous-time quantum Monte Carlo method as an impurity solver [14, 15, 40]. With DMFT + CT-QMC, quasiparticle weight, spectral weight, double occupancy, energy density, coefficient of specific heat are obtained. We presented those dynamical quantities for the half-filling case with semicirular density of states without symmetry breaking. We analyzed the physical content of those dynamical quantities, for example, we calculated the quasiparticle weight, extracted the critical electron-electron repulsion U_{c2} where the Metal-Mott insulator transition occurs. In all observable, we found that the metal-Mott insulator transition are the same. The metallic state far from the transition is well described by the Fermi liquid theory. As the temperature decreases, the critical U increases *i.e.*, the critical U is essentially temperature dependent which indicates that the entropies of metallic and insulating states are different. All observable in insulating phase are independent of temperature.

Chapter 5

Hubbard-Holsten Model

5.1 Introduction

Over the last years, tremendous progress have been made in the study of strongly correlated materials [11, 66], which typically contain partially filled and relatively localized $3d$, $4f$ or $5f$ orbitals. The low-energy physics of these materials can be described by an effective model Hamiltonian such as Hubbard, which is a minimal model to study strongly correlated electron systems. One of the fascinating phenomena of strongly correlated electron systems is correlation-driven Mott-Hubbard Metal-insulator transition. This transition from a paramagnetic metal to a paramagnetic insulator is found in various transition metal oxides, such as V_2O_3 doped with Cr, without change of crystal symmetry [67] (see Refs. within [67]). The single band Hubbard Hamiltonian with on-site electron-electron interaction U for example is believed to capture the physics of Mott-Hubbard metal- insulator [see chapter 4].

While the physics of materials with correlated electron systems is one of the most interesting and exciting topics, several classes of interesting materials exhibit an interplay of strong electron-electron Coulomb repulsion and strong electron-phonon coupling. Such interplay will be important to the problems such as the effects of phonons in the strongly correlated electron systems and the effects of electron correlations in

the electron-phonon coupled systems. These classes of materials include the cuprates [68, 69], alkali-doped fullerides [70, 71], manganites [72, 73] and the transition metal oxides [58], among others. The prototype model for describing such interplay is Holstein-Hubbard model. The model incorporates a coupling between electrons and dispersionless (i.e., Einstein) phonons with energy ω_0, in addition to the on-site Hubbard interaction U.

Several studies have already shown that the Hubbard-Holstein model treated within DMFT in combination with an exact diagonalization method [54, 56, 57] or within DMFT in combination with a numerical renormalization group method [54, 55, 74] successfully describes many properties of the electron-phonon interaction in strongly correlated electron systems. For example the effect of electron-phonon coupling on Mott-Hubbard metal-insulator transitions, a zero temperature phase diagram of symmetry unbroken states at half-filling.

5.2 Formalism

In this chapter we consider single band Hubbard-Holstein model which allows us to describe and explore the interplay of electron-electron and electron-phonon interactions. The Hubbard-Holstein is given by

$$\begin{aligned} H &= \sum_{\langle i,j\rangle\sigma} t_{ij}[d^{\dagger}_{i\sigma}d_{j\sigma} + d_{i\sigma}d^{\dagger}_{j\sigma}] - \mu\sum_{i}[n_{i\uparrow}+n_{i\downarrow}] + U\sum_{i} n_{i\uparrow}n_{i\downarrow} \\ &+ \lambda\sum_{i}(b^{\dagger}_{i}+b_i)(n_{i\uparrow}+n_{i\downarrow}-1) + \omega_0\sum_{i} b^{\dagger}_{i}b_i, \end{aligned} \tag{5.1}$$

where i, j denotes sites, σ is the spin, and the first sum is over nearest neighbors. $d^{\dagger}_{i,\sigma}$ denotes a creation operator of an electron, $b^{\dagger}_{i}$ is a creation operator of a phonon, t_{ij} is the hopping parameter, U is the on-site electron-electron interaction, μ is the chemical potential, λ is the coupling constant between electrons and phonons, and ω_0 is the phonon frequency

The original lattice enters in the calculation only through the density of states, which we always choose to be a semicircular one of half-bandwidth D (obviously $W = 2D = 4t$). For the one-band Hubbard-Holstein model with the semicircular density of states (Bethe lattice), and half-bandwidth D, the DMFT self-consistent Anderson impurity model has the following non-interacting Green's function:

$$\mathcal{G}_0^{-1}(\omega) = \omega + \mu - (D/2)^2 G(\omega) \tag{5.2}$$

where $G(\omega)$ is the local Green's functions.

Here we employ single-site DMFT, with a continuous-time quantum Monte Carlo (CT-QMC) based on the hybridization expansion (CT-HYB) impurity solver in the presence of retarded interaction. While there have been several work discussing the interplay of electron-electron and electron-phonon interactions at zero temperature in the Hubbard-Holstein model [34, 40, 46], the present work attempts to directly treat these interplay at non-zero temperature with single-site DMFT + CT-QMC.

5.3 Results and Discussion

5.3.1 Quasi-particle and Spectral weights at the Fermi level

In the context of quantum Monte Carlo simulations, one usually approximates the quasiparticle weight Z by

$$Z = \frac{1}{1 - \frac{Im\Sigma(i\omega)}{\omega_0}}. \tag{5.3}$$

Usually one always define the spectral weight $A(\omega = 0)$ at Fermi energy from the Green's function in imaginary time τ

$$\frac{\beta}{\pi} G(\tau = \beta/2) = \frac{\beta}{\pi} \int d\omega \frac{A(\omega)}{2\cosh(\beta\omega/2)} \longrightarrow A(\omega = 0) \qquad as \qquad T \longrightarrow 0, \tag{5.4}$$

to determine the critical interaction U_c for the metal-Mott insulator transition in continuous-time quantum Monte Carlo simulations. This is done in order to avoid the performance of an analytical continuation, which will produce some uncertainties.

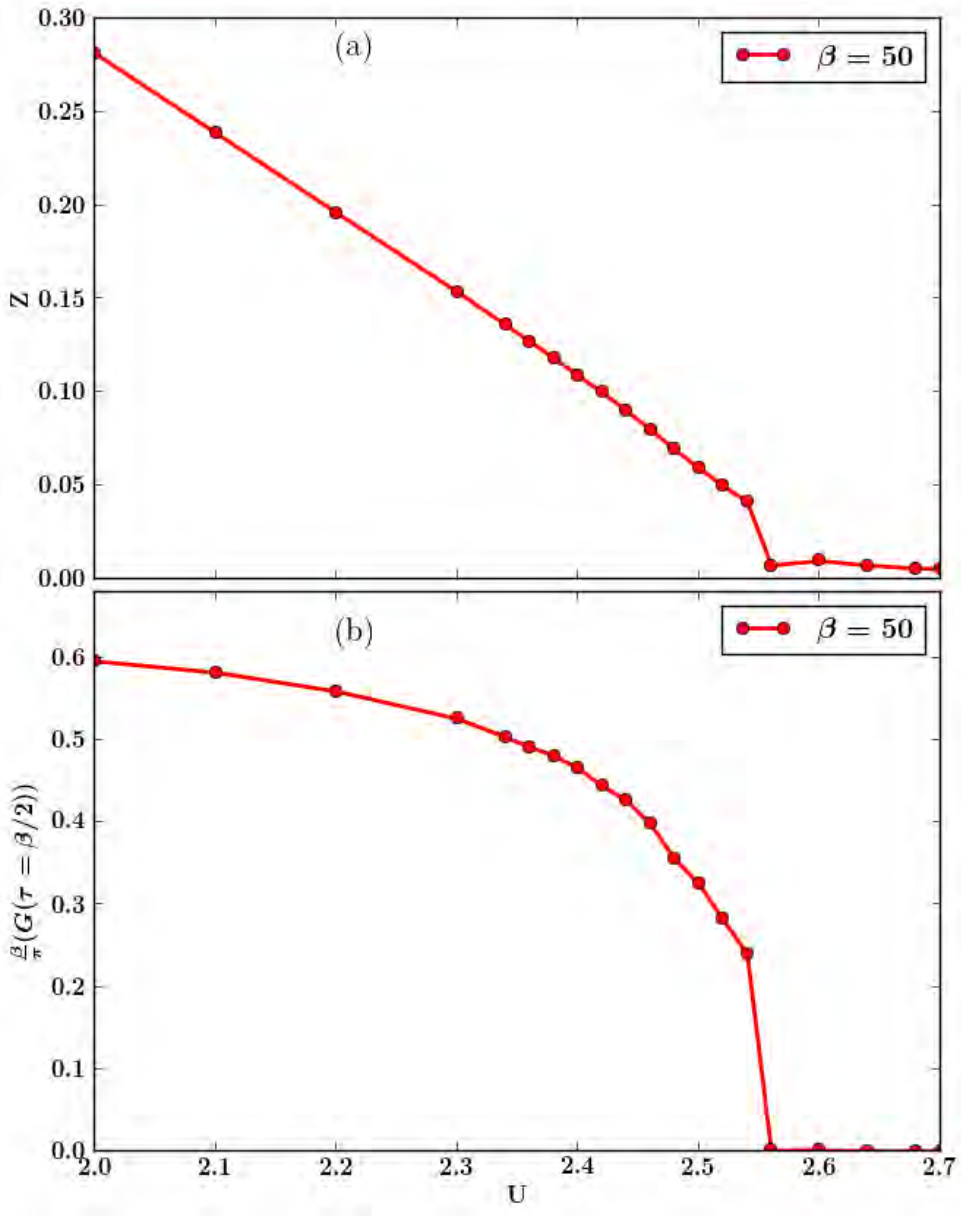

Fig. 5.1 The quasi-particle weight Z and spectral weight $\frac{\beta}{\pi}G(\tau = \beta/2)$ as a function of electron-electron repulsion U for value of electron-phonon coupling $\lambda = 0.2$ and phonon frequency $\omega_0 = 0.2$.

To see the effect of electron-phonon coupling on the Mott transition, we consider the variation of the quasiparticle weight and spectral weight at a fixed electron-phonon coupling λ. In figure (5.1 (a) we look at the cases $\lambda = 0.2$, and $\omega_0 = 0.2$. Upon increasing the on-site electron-electron interaction U, Z decreases, and the metal-Mott insulator transition occurs at around $U_{c2} \approx 2.56$. The effect of electron-phonon couplings results in the shift of metal-Mott insulator transition to larger values of the on-site electron-electron interaction. For example, the metal-Mott insulator transition in absence of electron-phonon coupling (Hubbard model) is $U_{c2} \approx 2.50$ [see chapter 4] where as in the presence of electron-phonon coupling is $U_{c2} \approx 2.56$.

Figure 5.1 (b) show the spectral weight as a function of electron-electron repulsion U for value of electron-phonon coupling $\lambda = 0.2$. The metal-Mott insulator occurs around $U_{c2} \approx 2.56$ as in the for quasiparticle weight Z.

5.3.2 Double Occupancy

The double occupancy $D = \langle n_{i\uparrow} n_{i\downarrow} \rangle$ are measured directly form the continuous-time quantum Monte Carlo and used to analyze phase transitions. To see whether the phase transition is first order or no we plot double occupancy as a function of the on-site electron-electron interaction U as shown in Fig. 5.2. The double occupancy has a jump behavior around the critical interaction $U_{c2} \approx 2.56$ which is an indication for the first order phase transition. However, the coexistence region become narrower as the electron-phonon coupling constant λ increases [34]

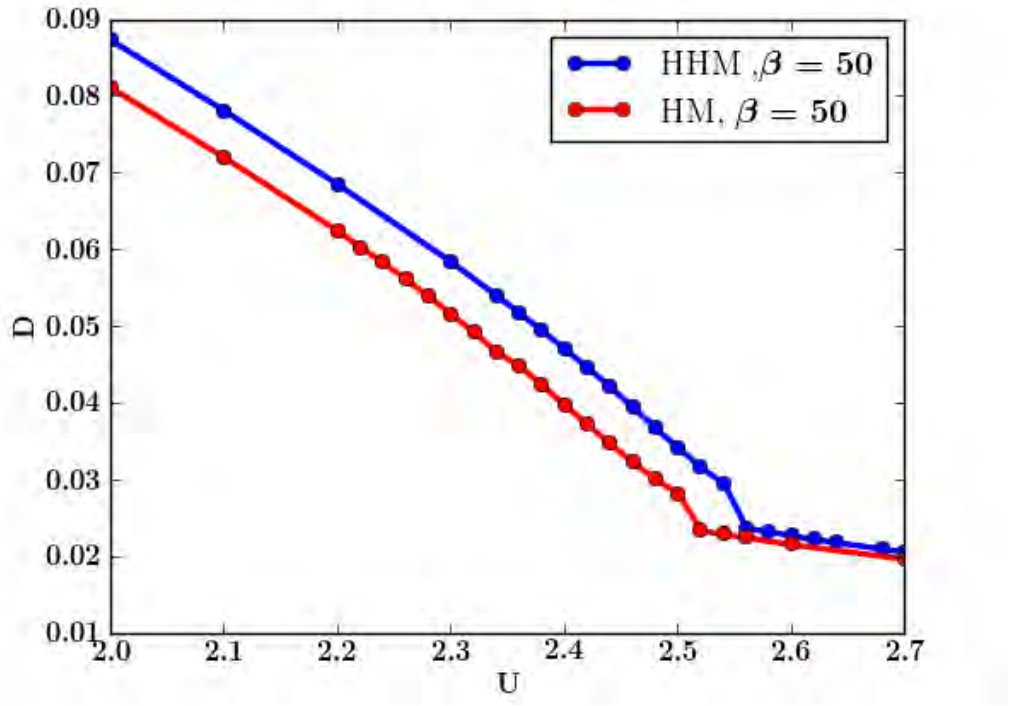

Fig. 5.2 Double occupancy D versus electron-electron interaction U for Hubbard model and Hubbard-Holstein model ($\lambda = 0.2$, and $\omega_0 = 0.2$) at temperature $T = 1/50$.

5.3.3 Linear Coefficient of Specific Heat

Here again, we estimate the linear coefficient of the specific hear γ for Hubbard-Holstein model from the density of states $A(\omega = 0)$ at the Fermi energy and quasiparticle weight Z by

$$\gamma = \frac{2\pi k_B^2}{3} \frac{A}{Z}. \tag{5.5}$$

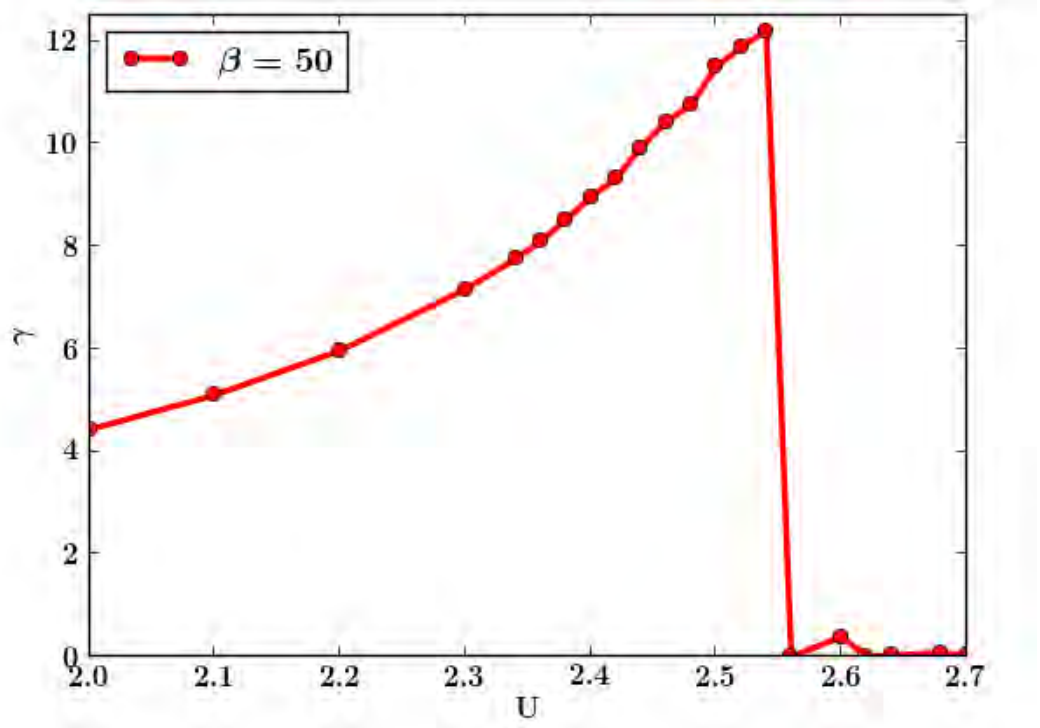

Fig. 5.3 Coefficient of heat capacity γ versus on-site electron-electron interaction U at electron-phonon coupling $\lambda = 0.2$, Einstein phonon frequency $\omega_0 = 0.2$ and temperature $T = 1/50$.

To see the effect of electron-phonon coupling constant λ in the strongly correlated electron systems we plot graph of coefficient of specific heat against the on-site electron-electron interaction U as shown in Fig. 5.3. The trends in Fig. 5.3 is identical to that of Hubbard model as shown in Fig. 4.4. However, there is a decrease in coefficient of specific heat for Hubbard-Holstein model as compared to the pure Hubbard model for the same on-site electron-electron interaction U. The decrease in coefficient of specific heat is attributed to the reduction of the on-site electron-electron interaction due to electron-phonon coupling constant λ. The other effect of electron-phonon coupling is the shift in metal-Mott insulator transition point to larger values of the on-site electron-electron interaction U.

5.3.4 Effect of electron-phonon interaction on correlated metal

For Hubbard-Holstein model give by Eq. (5.1), since the phonons are assumed to be noninteracting, one can integrate out the phonon part to drive the effective electron-electron interaction as [see Eqs. (2.50) and (2.51) of Chapter 2]

$$U_{eff}(i\omega) = U - \frac{2\lambda^2\omega_0}{\omega_0^2 - (i\omega)^2} \tag{5.6}$$

For static limit and for small frequencies compared to the characteristic frequency, the effective electron-electron interaction is

$$U_{eff} = U - \frac{2\lambda^2}{\omega_0} \tag{5.7}$$

Here we look at the dependence on electron-phonon coupling constant λ of the double occupancy, quasiparticle weight Z, kinetic energy E_{kin}, and coefficient of specific heat γ in the correlated metallic phase, in the region where the metal has not yet developed polaronic features.

Fig. 5.4 (a) show the effect of electron-phonon coupling constant λ on normalized double occupancy for different values of on-site electron-electron interaction U. For weakly correlated matal increasing electron-phonon coupling results in slightly increase of normalized double occupancy as long as $U_{eff} > 0$ but rapidly increases for $U_{eff} < 0$. possibly due to the formation of polaron crosover. However, for strongly correlated metal (for example $U = 2.4$), the effect of increasing electron-electron coupling results in enhancement of normalized double occupancy which is attributed to the screening of the on-site Hubbard electron-electron repulsion by electron-phonon interaction.

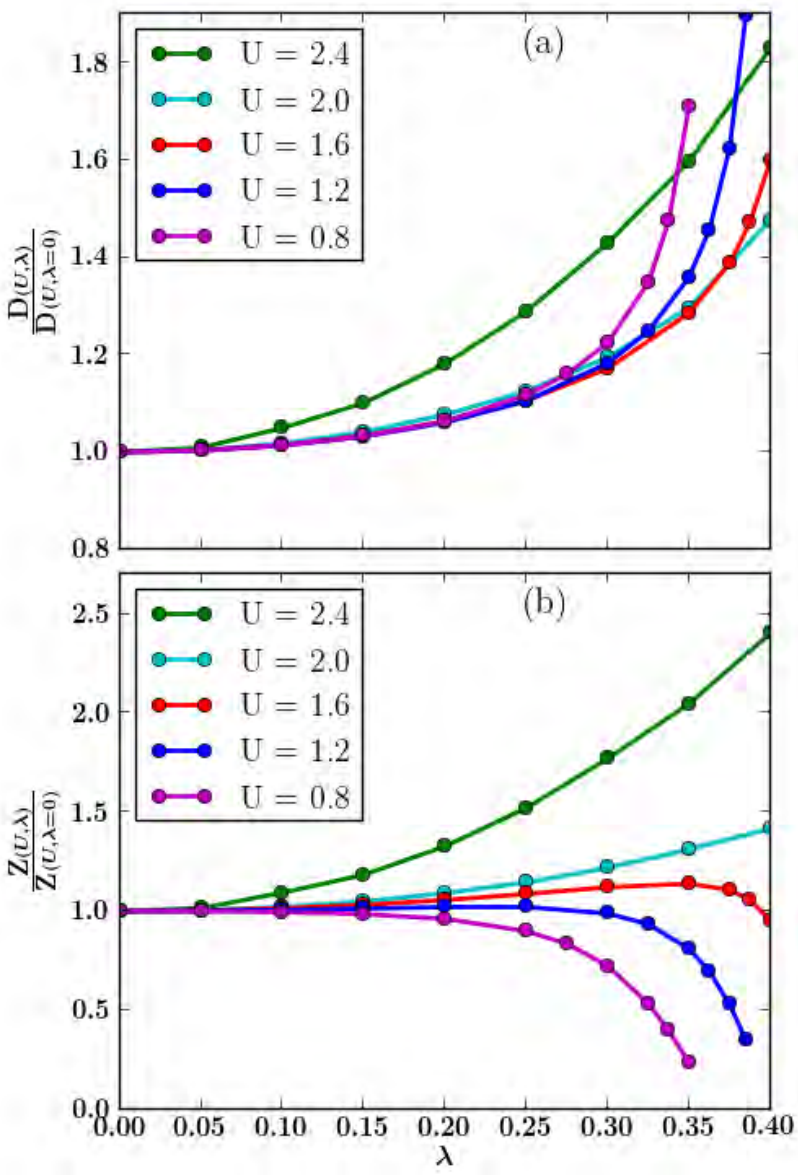

Fig. 5.4 Normalized double occupancy (a), Normalized quasiparticle weight Z (b) as a function of electron-phonon coupling constant λ for different values of on-site electron-electron interaction U and local Einstein phonon frequency $\omega_0 = 0.2$.

Figure 5.4 (b) show the normalized quasiparticle weight Z as a function of electron-phonon coupling constant λ for different values of on-site electron-electron interaction U. For weakly correlated metal in the region where $U_{eff} > 0$, the increase of electron-phonon coupling constant λ cause a little change in normalized quasiparticle weight Z. But for $U_{eff} < 0$ within the indicated electron-phonon coupling constant λ,

the normalized quasiparticle weight decreases (which corresponds to the enhancement of effective mass) as electron-phonon coupling constant λ increases. The enhancement of effective mass unfavorable the motion of electrons. This effect is attributed to the formation of polaron crossover.

However, for highly correlated metal close to metal-Mott insulator transition the increment of electron-phonon coupling constant λ results in the enhancement of quasiparticle weight Z (reduction of effective mass) This effect favors the motion of electrons by screening the Hubbard on-site electron-electron repulsion (as long as $U > 2\lambda^2/\omega_0$). The overall results of Fig. 5.4 (b) is in good agreement with the results found with the Numerical Renormalization Group and Exact Diagonalization solutions of DMFT in Ref. [54, 57].

Fig. 5.5 (b) below show the normalized potential energy as a function of electron-phonon coupling constant λ for different values of on-site electron-electron interaction U. For weakly correlated metal in the region where $U_{eff} > 0$, the increment of electron-phonon coupling constant λ results in a little change in potential energy. But there is an increment of potential energy as λ increases for $U_{eff} > 0$. For highly correlated metal, increasing electron-phonon coupling constant results in enhancement of potential energy as for double occupancy in Fig. 5.4 (a), since potential energy $E_{pot} = DU$.

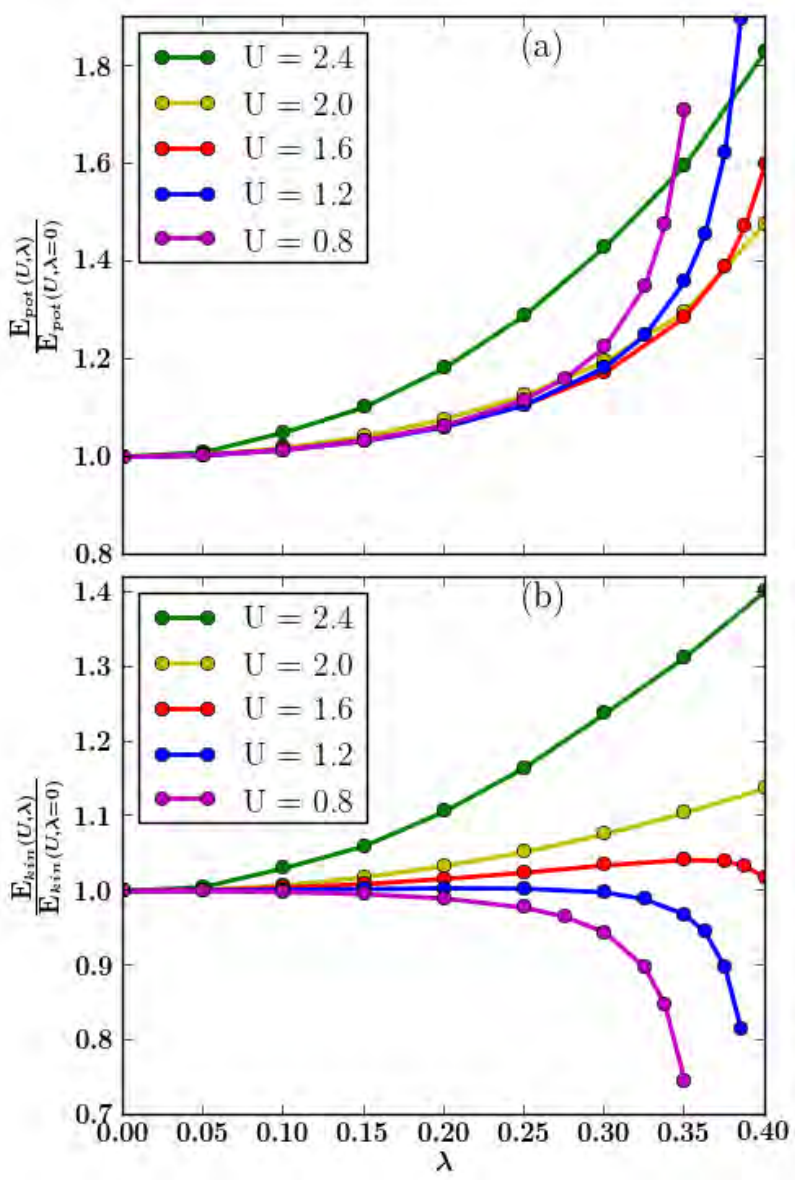

Fig. 5.5 Normalized Potential energy (a), and Normalized kinetic energy (b) as a function of electron-phonon coupling constant λ for different values of on-site electron-electron interaction U and local Einstein phonon frequency $\omega_0 = 0.2$.

To see the effect of electron-phonon coupling constant on correlated metal in more detail, we plot graph of Normalized kinetic energy as a function of electron-phonon coupling constant λ for different on-site electron-electron interaction U as shown in Fig. 5.5 (b) above. For weakly correlated metal in the region where $U_{eff} > 0$, increasing electron-phonon coupling λ causes a little effect in normalized kinetic energy. But in

the region where $U_{eff} < 0$, increasing the electron-phonon coupling constant λ causes the normalized kinetic energy to decrease significantly. This effect could be attributed to the formation of polaron/ bipolaron which could decreases the kinetic energy.

However, for highly correlated metal close to metal-Mott insulator transition (for example $U = 2.4$) increasing the electron-phonon coupling constant λ results in the enhancement of kinetic energy for $U_{eff} > 0$. This effect favors the fluctuation of charges by screening the Hubbard on-site electron-electron repulsion, which intern results in the enhancement of kinetic energy. The increase in kinetic energy here is consistent with the enhancement of quasiparticle wight Z, as show in Fig. 5.4 (b), with the same parameters.

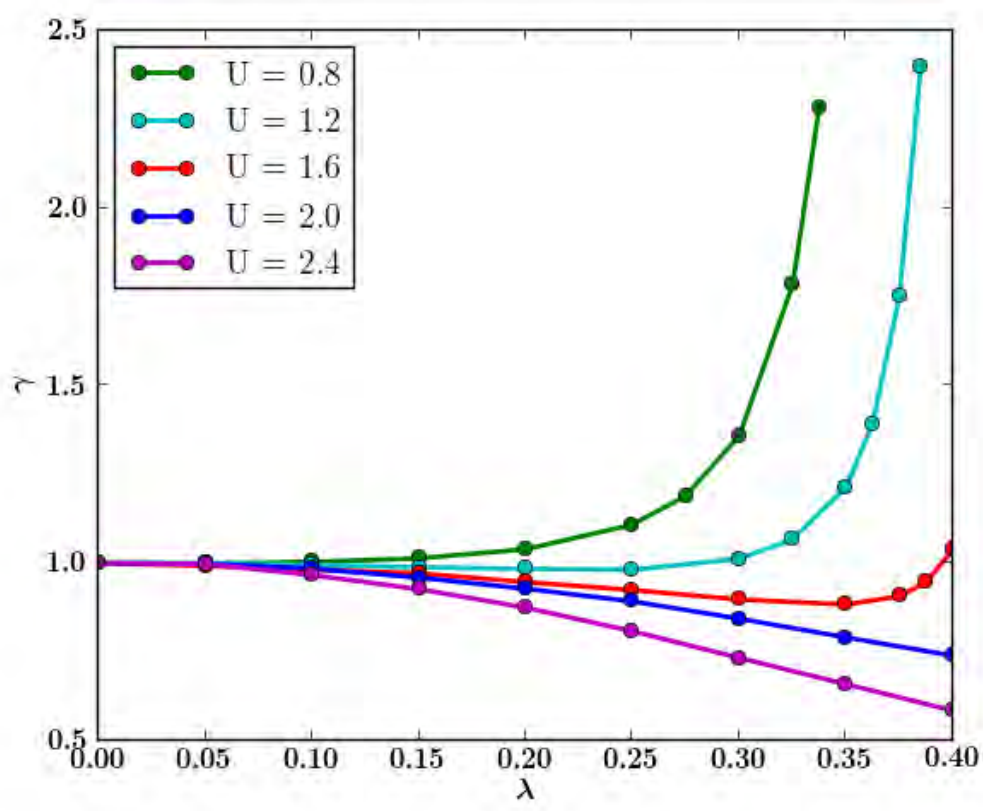

Fig. 5.6 Coefficient of heat capacity γ versus electron-phonon coupling constant λ for different values of on-site electron-electron interaction U, Einstein phonon frequency $\omega_0 = 0.2$ at temperature $T = 1/50$.

Fig. 5.6 above shows the coefficient of specific heat versus electron-phonon coupling constant λ for different values of on-site electron-electron interaction U. For weakly correlated metal in the region where $U_{eff} = U - 2\lambda^2/\omega_0 > 0$, increasing electron-phonon coupling λ has a little effect on coefficient of specific heat. But increasing electron-phonon coupling in the region where $U_{eff} < 0$ causes the coefficient of specific heat to increase, which is in line with the result we found in Fig. 5.4 (b), where the effective mass is enhanced [$\gamma \propto m^*$].

However, for highly correlated metal close to metal-Mott insulator transition where $U_{eff} > 0$, increasing electron-phonon coupling constant λ causes a little effect on coefficient of specific heat as the repulsive electron-electron interaction U_{eff} effectively suppresses charge fluctuations which would otherwise couple to the phonons. This is in good agreement with our finding of Fig. 5.4 (b) where the quasiparticle weight Z is enhanced.

Therefore it is clear from Figs. (5.4, 5.5, 5.6) that, within the Hubbard-Holstein model, the effect of electron-phonon coupling constant λ depends on the value of the Hubbard electron-electron repulsion U (whether the material is strongly correlated or weakly correlated).

5.4 Conclusion

We have studied the interplay of electron-electron and electron-phonon coupling in single band Hubbard-Holstein model on Bethe lattice using single-site dynamical mean field theory (DMFT), which is exact in infinite spatial dimensions, with continuous-time quantum Monte Carlo (CT-QMC) method as impurity solver [14, 15, 40]. With DMFT + CT-QMC, quasiparticle wight, spectral weight,double occupancy, energy density, coefficient of specific heat are obtained. We present those dynamical quantities for half-filling case with semicircular density of states without symmetry breaking. We analyzed the physical content of those dynamical quantities, for example, we calculated

the quasiparticle weight, extracted the critical electron-electron repulsion U_{c2} where the Metal-Mott insulator transition occurs. The effect of electron-phonon coupling constant λ in Hubbard-Holstein model shifts the metal-Mott insulator transition to a larger values as compared to the pure Hubbard model and the transition remain first order.

Furthermore, we address the effect of electron-phonon coupling on correlated metals. Our result indicates that the effect of electron-phonon coupling under Hubbard-Holstein model depends on the values of Hubbard electron-electron repulsion U.

Chapter 6

Summery and Conclusion

In this thesis, we analyzed the single-band Hubbard Model and single-band Hubbard-Holstein band at half-filling in the limit of infinite dimension. In this limit, the full lattice Hamiltonian can be mapped on a single impurity Anderson model which we solved by the continuous-time quantum Monte Carlo (CT-QMC).

The first part of our work devoted on correlation driven metal-Mott insulator transition and properties of this correlated electron systems around the metal-Mott insulator transition. We used the Hubbard model, which is the minimal model to study strongly correlated electron systems, on Bethe lattice with out symmetry breaking, whose density of state is semicircular. With the DMFT + CT-QMC method, we measured dynamical quantities such as, Green's functions, self-energy, density-density correlation functions, average expansion order. Based on the physical content of these dynamical quantities, for example, we calculated the quasiparticle weight, spectral weight, double occupancy, and extracted the critical electron-electron repulsion U_{c2} where the metal-Mott insulator transition occurs. All calculated dynamical quantities indicate the same critical repulsion U_{c2} where metal-Mott insulator transition occurs. The metallic state far from the transition is well described by the Fermi liquid theory. As the temperature decreases, the critical U increases *i.e.*, the critical U is essentially

temperature dependent which indicates that the entropies of metallic and insulating states are different. All observable in insulating phase are independent of temperature.

The second part of our work is effect of electron-phonon coupling on correlation driven metal-Mott insulator transition and on correlated metal. We used the Hubbard-Holstein model, which is the minimal model to study the interplay of electron-electron interactions and electron-phonon interaction, on Bethe lattice with out symmetry breaking, whose density of state is semicircular. With the DMFT + CT-QMC method, in the presence of retarded interaction, we measured dynamical quantities such as, Green's functions, self-energy, density-density correlation functions, average expansion order. Based on the physical content of these dynamical quantities, for example, we calculated the quasiparticle weight, spectral weight, double occupancy, and extracted the critical electron-electron repulsion U_{c2} where the metal-Mott insulator transition occurs. The effect of electron-phonon coupling on correlation driven metal-Mott insulator transition is shifting the critical repulsion U_{c2} metal-Mott insulator transition to larger values. Furthermore, we address that the effect of electron-phonon coupling depends on the values of on-site electron-electron interaction U.

References

[1] F. Lechermann, Model Hamiltonians and Basic Techniques, in *The LDA+DMFT approach to strongly correlated materials*, edited by E. Pavarini, E. Koch, D. Vollhardt, and A. Lichtenstein, volume 1, Forschungszentrum Jülich GmbH, Germany, 2011.

[2] M. Born and R. Oppenheimer, Zur Quantentheorie der Molekeln, Annalen der Physik **389**, 457 (1927).

[3] W. Kohn, Nobel Lecture: Electronic structure of matter—wave functions and density functionals, Reviews of Modern Physics **71**, 1253 (1999).

[4] P. Hohenberg and W. Kohn, Inhomogeneous Electron Gas, Phys. Rev. **136**, B864 (1964).

[5] W. Kohn and L. J. Sham, Self-Consistent Equations Including Exchange and Correlation Effects, Phys. Rev. **140**, A11330 (1965).

[6] G. A. Sawatzky and J. W. Allen, Magnitude and Origin of the Band Gap in NiO, Phys. Rev. Lett. **53**, 2339 (1984).

[7] V. I. Anisimov, I. V. Solovyev, M. A. Korotin, M. T. Czyżyk, and G. A. Sawatzky, Density-functional theory and NiO photoemission spectra, Phys. Rev. B **48**, 16929 (1993).

[8] J. Hubbard, Electron Correlations in Narrow Energy Bands, Proceedings of the Royal Society of London. Series A, Mathematical and Physical Sciences **276**, 238 (1963).

[9] N. F. Mott, *Metal-Insulator Transitions*, Taylor and Francis, 1990.

[10] F. Gebhard, *The Mott Metal-Insulator Transition : Models and Methods*, Springer, New York, 1997.

[11] A. Georges, G. Kotliar, W. Krauth, and M. J. Rozenberg, Dynamical mean field theory of strongly correlated fermion systems and the limit of infinite dimensions, Rev. Mod. Phys. .

[12] J. E. Hirsch and R. M. Fye, Monte Carlo Method for Magnetic Impurities in Metals, Phys. Rev. Lett. **56**, 2521 (1986).

[13] A. N. Rubtsov, V. V. Savkin, and A. I. Lichtenstein, Continuous-time quantum Monte Carlo method for fermions, Phys. Rev. B **72**, 035122 (2005).

[14] P. Werner, A. Comanac, L. de' Medici, M. Troyer, and A. J. Millis, Continuous-time solver for quantum impurity models, Phys. Rev. Lett. **97**, 076405 (2006).

[15] P. Werner and A. J. Millis, Hybridization expansion impurity solver: General formulation and application to kondo lattice and two-orbital models, Phys. Rev. B **74**, 155107 (2006).

[16] M. C. Gutzwiler, Effect of Correlation on the Ferromagnetism of Transition Metals, Phys. Rev. Lett. **10**, 159 (1963).

[17] J. Kanamori, Electron correlation and ferromagnetism of transition metals, Progress of Theoretical Physics **30**, 3296 (1963).

[18] H. Tasaki, The Hubbard model - an introduction and selected rigorous results, Journal of Physics: Condensed Matter **10**, 4353 (1998).

[19] E. H. Lieb and F. Wu, Absence of Mott Transition in an Exact Solution of the Short-Range, One-Band Model in One Dimension, Phys. Rev. Lett. **20**, 1445 (1968).

[20] M. Kollar, Introduction to DynamicalMean-Field Theory, in *The LDA+DMFT approach to strongly correlated materials*, edited by E. Pavarini, E. Koch, D. Vollhardt, and A. Lichtenstein, Forschungszentrum Jülich GmbH Institute for Advanced Simulaton (IAS), Germany, 2011.

[21] P. W. Anderson, New Approach to the Theory of Superexchange Interactions, Phys. Rev. **115**, 2 (1959).

[22] J. Spałek, Effect of pair hopping and magnitude of intra-atomic interaction on exchange-mediated superconductivity, Phys. Rev. B **37**, 533 (1988).

[23] N. F. Mott, The Basis of the Electron Theory of Metals, with Special Reference to the Transition Metals, Proc. Phys. Soc. A **49**, 72 (1949).

[24] J. H. de Boer and E. J. W. Verwey, Semi-conductors with partially and with completely filled 3d-lattice bands, Proceedings of the Physical Society **49**, 39 (1937).

[25] W. F. Brinkman and T. M. Rice, Application of Gutzwiller's Variational Method to the Metal-Insulator Transition, Phys. Rev. B **2**, 4302 (1970).

[26] W. Metzner and D. Vollhardt, Correlated Lattice Fermions in $d = \infty$ Dimensions, Phys. Rev. Lett. **62**, 324 (1989).

[27] E. Müller-Hartmann, Correlated fermions on a lattices in high dimensions, Z. Phys. B **74**, 507 (1989).

[28] E. Müller-Hartmann, The Hubbard model at high dimensions: some exact results and weak coupling theory, Z. Phys. B **76**, 211 (1989).

[29] A. Georges and G. Kotliar, Hubbard model in infinite dimensions, Phys. Rev. B **45**, 6479 (1992).

[30] K. Held, Electronic structure calculations using dynamical mean field theory, Advances in Physics **56**, 829 (2007).

[31] J. W. Negele and H. Orland, *Quantum Many-Particle Systems*, Addison-Wesley, 1998.

[32] K. Byczuk and D. Vollhardt, Correlated bosons on a lattice: Dynamical mean-field theory for Bose-Einstein condensed and normal phases, Phys. Rev. B **77**, 235106 (2008).

[33] A. Hubener, M. Snoek, and W. Hofstetter, Magnetic phases of two-component ultracold bosons in an optical lattice, Phys. Rev. B **80**, 245109 (2009).

[34] P. Werner and A. J. Millis, Dynamical Screening in Correlated Electron Materials, Phys. Rev. Lett. **104**, 146401 (2010).

[35] H. Hafermann, Self-energy and vertex functions from hybridization-expansion continuous-time quantum Monte Carlo for impurity models with retarded interaction, Phys. Rev. B **89**, 235128 (2014).

[36] P. W. Anderson, Localized Magnetic States in Metals, Phys. Rev. **124**, 41 (1961).

[37] R. Bulla, T. A. Costi, and T. Pruschke, Numerical renormalization group method for quantum impurity systems, Rev. Mod. Phys **80**, 395 (2008).

[38] K. G. Wilson, The renormalization group: Critical phenomena and the Kondo problem, Rev. Mod. Phys **47**, 773 (1975).

[39] M. Caffarel and W. Krauth, Exact diagonalization approach to correlated fermions in infinite dimensions: Mott transition and superconductivity, Phys. Rev. Lett **72**, 1545 (1994).

[40] E. Gull, A. J. Millis, A. I. Lichtenstein, A. N. Rubtsov, M. Troyer, and P. Werner, Continuous-time Monte Carlo methods for quantum impurity models, Revies of Modern Physics **83**, 349 (2011).

[41] R. N. Silver, D. S. Sivia, and J. E. Gubernatis, Maximum-entropy method for analytic continuation of quantum Monte Carlo data, Phys. Rev. B **41**, 2380 (1990).

[42] M. Jarrell and J. E. Gubernatis, Bayesian inference and the analytic continuation of imaginary-time quantum Monte Carlo data, Physics Reports **269**, 133 (1996).

[43] E. Gull, P. Werner, A. Millis, and M. Troyer, Performance analysis of continuous-time solvers for quantum impurity models, Phys. Rev. B **76**, 235123 (2007).

[44] J. Otsuki, H. Kusunose, P. Werner, and Y. Kuramoto, Continuous-Time Quantum Monte Carlo Method for the Coqblin-Schrieffer Model, J. Phys. Soc. Jpn **76**, 114707 (2007).

[45] S. Hoshino, J. Otsuki, and Y. Kuramoto, Continuous-Time Quantum Monte Carlo Approach to Singlet–Triplet Kondo Systems, J. Phys. Soc. Jpn **78**, 074719 (2009).

[46] P. Werner and A. J. Millis, Efficient Dynamical Mean Field Simulation of the Holstein-Hubbard Model, Phys. Rev. Lett. **99**, 146404 (2007).

[47] B. Bauer, L. D. Carr, H. G. Evertz, A. Feiguin, J. Freire, S. Fuchs, L. Gamper, J. Gukelberger, E. Gull, S. Guertler, A. Hehn, R.Igarashi, S. V. Isakov, D. Koop, P. Ma, P. Mates, H. Matsuo, O. Parcollet, G. Pawlowski, J. D. Picon, L. Pollet, E. Santos, V. W. Scarola, U. Schollwock, C. Silva, B. Surer, S. Todo, S. Trebst, M. Troyer, M. L. Wall, P. Werner, and S. Wessel, The ALPS project release 2.0: open source software for strongly correlated systems, Journal of Statistical Mechanics: Theory and Experiment **05/P05001**, 1742 (2011).

[48] H. Hafermann, P. Werner, and E. Gull, Efficient implementation of the continuous-time hybridization expansion quantum impurity solver, Computer Physics Communications **184**, 1280 (2013).

[49] P. Werner, Continuous-Time Impurity Solvers, in *The LDA+DMFT approach to strongly correlated materials*, edited by E. Pavarini, E. Koch, D. Vollhardt, and A. Lichtenstein, Forschungszentrum Jülich GmbH Institute for Advanced Simulaton (IAS), Germany, 2011.

[50] E. Gull, *Continuous-Time Quantum Monte Carlo Algorithms for Fermions*, PhD thesis, ETH ZURICH, 2008.

[51] N. Metropolis, A. W. Rosenbluth, M. N. Rosenbluth, A. H. Teller, and E. Teller, Equation of State Calculations by Fast Computing Machines, J. Chem. Phys **21**, 1087 (1953).

[52] W. K. Hastings, Monte Carlo sampling methods using Markov chains and their applications, Biometrika **57**, 97 (1970).

[53] M. Troyer and U. Wiese, Computational Complexity and Fundamental Limitations to Fermionic Quantum Monte Carlo Simulations, Phys. Rev. Lett **94**, 170201 (2005).

[54] W. Koller, D. Meyer, Y. Ono, and A. C. Hewson, First-and second-order phase transitions in the Holstein-Hubbard model, Europhysics lett. **66**, 559 (2004).

[55] W. Koller, A. C. Hewson, and D. M. Edwards, Polaronic Quasiparticles in a Strongly Correlated Electron Band, Phys. Rev. Lett **95**, 256401 (2005).

[56] M. Capone, G. Sangiovanni, C. Castellani, C. D. Castro, and M. Grilli, Phase Separation Close to the Density-Driven Mott Transition in the Hubbard-Holstein Model, Phys. Rev. Lett. **92**, 106401 (2004).

[57] G. Sangiovanni, M. Capone, C. Castellani, and M. Grilli, Electron-Phonon Interaction Close to a Mott Transition, Phys. Rev. Lett. **94**, 026401 (2005).

[58] M. Imada, Metal-insulator transitions, Rev. Mod. Phys. **70**, 1039 (1998).

[59] P. Limelette1, A. Georges, D. Jerome1, P. Wzietek, P. Metcalf3, and J. M. Honig, Universality and Critical Behavior at the Mott Transition, Science **302**, 89 (2003).

[60] J. C. Slator, Magnetic effects and the Hartree-Fock equation, Phys, Rev. **82**, 538 (1951).

[61] R. Bulla, T. A. Costi, and D. Vollhardt, Finite-temperature numerical renormalization group study of the Mott transition, Phys. Rev. B **64**, 045103 (2001).

[62] A. Liebsch, Mott Transitions in Multiorbital Systems, Phys. Rev. Lett. **92**, 226401 (2002).

[63] N. Blümer, *Mott-Hubbard Metal-Insulator Transition and Optical Conductivity in High Dimensions*, PhD thesis, Universitäte Augsburg, 2002.

[64] A. J. Kim, M. Y. Choi, and G. S. Jeon, Estimate of the phase transition line in the infinite-dimensional Hubbard model, Journal of the Korean Physical Society **64**, 268 (2014).

[65] C. A. Marianetti, K. Haule, and O. Parcollet, Quasiparticle Dispersion and Heat Capacity of $Na_{0.3}CoO_2$: A Dynamical Mean Field Theory Study, Phys. Rev. Lett. **99**, 246404 (2007).

[66] G. Kotliar, S. Y. Savrasov, K. Haule, V. S. Oudovenk, O. Parcollet, and C. A. Marianetti, Electronic structure calculations with dynamical mean-field theory, Rev. Mod. Phys. **70**, 865 (2006).

[67] I. Leonov, V. I. Anisimov, and D. Vollhardt, Metal-insulator transition and lattice instability of paramagnetic V_2O_3, Phys. Rev. B **91**, 195115 (2015).

[68] A. Lanzara, P. V. Bogdanov, X. J. Zhou, S. A. Kellar, D. L. Feng, E. D. Lu, T. Yoshida, H. Eisaki, A. Fujimori, K. Kishio, J. I. Shimoyama, T. Noda, S. Uchida, Z. Hussain, and Z. X. Shen, Evidence for ubiquitous strong electron–phonon coupling in high-temperature superconductors, Nature **412**, 510 (2001).

[69] G. H. Gweon, T. Sasagawa, S. Zhou, J. Graf, H. Takagi, D. H. Lee, and A. Lanzara, An unusual isotope effect in a high-transition-temperature superconductor, Nature **420**, 187 (2004).

[70] Y. Takabayashi, A. Y. Ganin, P. Jeglic, D. Arcon, T. Takano, Y. Iwasa, Y. Ohishi, M. Takata, N. Takeshita, K. Prassides, and M. J. Rosseinsky, The Disorder-Free Non-BCS Superconductor Cs_3C_{60} Emerges from an Antiferromagnetic Insulator Parent State, Science **323**, 1585 (2009).

[71] M. Capone, M. Fabrizio, C. Castellani, and E. Tosatti, Colloquium: Modeling the unconventional superconducting properties of expanded A_3C_{60} fullerides, Rev. Mod. Phys. **81**, 943 (2009).

[72] M. B. Salamon and M. Jaime, The physics of manganites: Structure and transport, Rev. Mod. Phys **73**, 583 (2001).

[73] A. J. Millis, Lattice effects in magnetoresistive manganese perovskites, Nature **392**, 147 (1998).

[74] G. S. Jeon, T.-H. Park, J. H. Han, H. C. Lee, and H.-Y. Choi, Dynamical mean-field theory of the Hubbard-Holestein model at half filling: Zero temperature meta-insulator and insulator-insulator transitions, Phys. Rev. B **70**, 125114 (2004).

Appendix A

Green's Function

In the context of quantum mechanics a propagator describes the propagation of a disturbance created by injection of a particle into a state at one time and its removal from another state at another time. We use here the finite-temperature Matsubara formalism. The quantity of interest for us is the fermionic single particle Green function

$$G_{ij}(\tau - \tau') = -\langle T_\tau d_{i,\sigma}(\tau) d^\dagger_{j,\sigma}(\tau') \rangle \tag{A.1}$$

Here τ is imaginary time, T_τ is the imaginary time ordering operator, $d_{i,\sigma}(\tau)(d^\dagger_{j,\sigma}(\tau'))$ are creation (annihilation) operators in imaginary time Heisenberg picture.

For free particles, with Hamiltonian $H - \mu N = \sum_{\mathbf{k},\sigma}(\varepsilon_{\mathbf{k}} - \mu) d^\dagger_{\mathbf{k},\sigma} d_{\mathbf{k},\sigma}$, the Fourier transformation of eq. $(A.1)$ reads as

$$G_{\mathbf{k}\sigma}(i\omega)^0 = \frac{1}{i\omega + \mu - \varepsilon_{\mathbf{k}}} \tag{A.2}$$

where $\varepsilon_{\mathbf{k}} = \sum_{ij} t_{ij} e^{i\mathbf{k}(\mathbf{R}_i - \mathbf{R}_j)}$ the dispersion relation.

For interacting systems the self-energy $\Sigma_{\mathbf{k}}(i\omega)$ is defined so that it measures the difference between interacting and free Green functions:

$$G_{\mathbf{k}}(i\omega_n) = \frac{1}{i\omega_n + \mu - \varepsilon_{\mathbf{k}} - \Sigma_{\mathbf{k}}(i\omega_n)} = \frac{1}{\left(\frac{1}{i\omega_n+\mu-\varepsilon_{\mathbf{k}}}\right)^{-1} - \Sigma_{\mathbf{k}}(i\omega_n)} = \frac{1}{(G^0_{\mathbf{k}}(i\omega_n))^{-1} - \Sigma_{\mathbf{k}}(i\omega_n)} \tag{A.3}$$

The lattice self-energy become local quantities in the limit of large dimensions. The lattice Green's function can therefore be written as

$$G_{\mathbf{k}} = \frac{1}{\eta - \varepsilon_{\mathbf{k}}}, \qquad \eta = i\omega_n + \mu - \Sigma(i\omega_n) \tag{A.4}$$

It is then straightforward to check the following identities for the Green's function

$$\sum_{\mathbf{k}} \varepsilon_{\mathbf{k}} G_{\mathbf{k}} = \sum_{\mathbf{k}} \frac{\varepsilon_{\mathbf{k}} - \eta + \eta}{\eta - \varepsilon_{\mathbf{k}}} = -1 + \eta \sum_{\mathbf{k}} G_{\mathbf{k}} = -1 + \eta G_{00} \tag{A.5}$$

$$\sum_{\mathbf{k}} \varepsilon^2_{\mathbf{k}} G_{\mathbf{k}} = \sum_{\mathbf{k}} \frac{\varepsilon_{\mathbf{k}}(\varepsilon_{\mathbf{k}} - \eta) + \varepsilon_{\mathbf{k}}\eta}{\eta - \varepsilon_{\mathbf{k}}} = \eta \sum_{\mathbf{k}} \frac{\varepsilon_{\mathbf{k}}}{\eta - \varepsilon_{\mathbf{k}}} = \eta + \eta^2 G_{00} \tag{A.6}$$

Appendix B

Functional Integral for quantum partition function

Much of the information on quantum many-particle systems is encoded in expectation value of products of creation and annihilation operators, i.e. expression of the structure $\langle c^{\dagger} c \cdots \rangle$. Objects of this type are generally called correlation functions. At any finite temperature the average $\langle \cdots \rangle$ entering the definition of correlation function runs over the quantum Gibbs distribution[31]

$$\hat{\rho} = \frac{e^{-\beta(\hat{H}-\mu\hat{N})}}{Z} \tag{B.1}$$

Where

$$Z = Tre^{-\beta(\hat{H}-\mu\hat{N})} = \Sigma_n \langle n|e^{-\beta(\hat{H}-\mu\hat{N})}|n\rangle \tag{B.2}$$

is the quantum partition function function, β=1/T, μ denotes the chemical potential, ans the sum extends over a complete set of Fock space $\{|n\rangle\}$. The closure relation of the coherent state is

$$\int \prod_{\alpha} dc_{\alpha}^{*} dc_{\alpha} e^{-\sum_{\alpha} c_{\alpha}^{*} c_{\alpha}} |c\rangle\langle c| = \hat{I} \tag{B.3}$$

From (Eq.B.2) and (Eq.B.3) and using $\prod_\alpha dc^*_\alpha c_\alpha = dc^*_\alpha dc_\alpha$

$$Z = \int d[c^*_\alpha c_\alpha] e^{-\sum_\alpha c^*_\alpha c_\alpha} \sum_n \langle n|c\rangle\langle c|e^{-\beta(\hat{H}-\mu\hat{M})}|n\rangle \tag{B.4}$$

Using the anti-commuting relation of fermionic $\langle n|c\rangle\langle c|n\rangle = \langle \eta c|n\rangle\langle n|c\rangle$, with η=-1, we have

$$Z = \int d[c^*_\alpha c_\alpha] e^{-\sum_\alpha c^*_\alpha c_\alpha} \langle \eta c|e^{-\beta(\hat{H}-\mu\hat{M})}|c\rangle \tag{B.5}$$

The Trotter decomposition to do Taylor expansion

$$\begin{aligned} e^{-\beta(\hat{H}-\mu\hat{N})} &= e^{[-\triangle\tau(\hat{H}-\mu\hat{N})]N} \\ &= \lim_{N\longrightarrow\infty} \prod (1-\triangle\tau(\hat{H}-\mu\hat{N})) \\ &= \lim_{N\longrightarrow\infty} \prod e^{-\triangle\tau(\hat{H}-\mu\hat{N})} \end{aligned} \tag{B.6}$$

where $\triangle\tau = \beta/N$. Inserting N-1 times the closure properties we have

$$Z = \int \prod_{k=1}^{N} d[c^*_k c_k] e^{-\sum_{k=1}^{N}\sum^*_{k,\alpha} c_{k,\alpha}} \prod_{k=1}^{N} \langle c_k|e^{-\triangle\tau(\hat{H}-\mu\hat{N})}|c_{k-1}\rangle \tag{B.7}$$

If the Hamiltinian $\hat{H} = H(c^\dagger_\alpha, c_\alpha)$ and $\hat{N} = \sum_\alpha c^\dagger_\alpha c_\alpha$ is the normal order

$$\begin{aligned} \langle c_k|e^{-\Delta\tau(\hat{H}-\mu\hat{N})}|c_{k-1}\rangle &= \langle c_k|1-\Delta\tau[H(c^\dagger_\alpha, c_\alpha) - \mu\sum_\alpha c^\dagger_\alpha c_\alpha]|c_{k-1}\rangle \\ &= \langle c_k|c_{k-1}\rangle e^{-\Delta\tau\sum_{k=1}^{N}\sum_\alpha [H(c^*_{k,\alpha}, c_{k-1,\alpha}) - \mu c^*_{k,\alpha} c_{k-1,\alpha}]} \\ &= e^{-\Delta\tau\sum_{k=1}^{N}\sum_\alpha c^*_{k,\alpha} c_{k-1.\alpha}} \\ &\times \ (e^{-\Delta\tau\sum_{k=1}^{N}\sum_\alpha [H(c^*_{k,\alpha}, c_{k-1,\alpha}) - \mu c^*_{k,\alpha} c_{k-1,\alpha}]}) \\ &= e^{-\Delta\tau\sum_{k=1}^{N}\sum_\alpha (c^*_{k,\alpha} c_{k-1,\alpha}[1-\Delta\tau\mu] - \Delta\tau H(c_{k,\alpha}.c_{k-1,\alpha}))} \end{aligned} \tag{B.8}$$

In view of equation (B.8, equation (B.7) becomes

$$Z = \int \prod_{k=1}^{N} d[c_k^*, c_k] exp(-\Delta\tau \sum_{k=1}^{N} c_{k,\alpha}^* [\frac{(c_{k,\alpha} - c_{k-1,\alpha})}{\triangle\tau} - \mu c_{k-1,\alpha}] + H(c_{k,\alpha}^*, c_{k-1,\alpha})) \tag{B.9}$$

For $\Delta\tau \longrightarrow 0$ and N $\longrightarrow \infty$, it is convenient to represent the set of $c_{0,\alpha}...c_{N,\alpha}$ by a continuous trajectory $c_\alpha(\tau)$ with τ an imaginary time varying between 0 and β.

$$\Delta\Sigma_{k=1}^{N} \longrightarrow \int d\tau \tag{B.10}$$

$$c_{k,\alpha}^* \frac{(c_{k,\alpha} - c_{k-1,\alpha})}{\Delta\tau} \longrightarrow c_\alpha^*(\tau)\partial_\tau c_\alpha(\tau) \tag{B.11}$$

$$H(c_{k,\alpha}, c_{k,\alpha}) \longrightarrow H(c_\alpha^*(\tau), c_\alpha(\tau)) \tag{B.12}$$

$$\lim_{N\longrightarrow\infty} \prod_{k=1}^{N} d[c^*, c] \longrightarrow D[c^*, c] \tag{B.13}$$

Using equations (B.10 - B.13), Eq. (B.9) becomes

$$Z = \int D[c^*, c] e^{(-\int_0^\beta d\tau [\sum_\alpha c_\alpha(\tau)(\partial_\tau - \mu)c_\alpha(\tau) + H(c_\alpha^*(\tau), c_\alpha(\tau)])} \tag{B.14}$$

and hence

$$Z = \int D[c^*, c] e^{[-S]} \tag{B.15}$$

Where the action S is

$$S = \int_0^\beta d\tau [\sum_\alpha c_\alpha(\tau)(\partial_\tau - \mu)c_\alpha(\tau) + H(c_\alpha^*(\tau), c_\alpha(\tau)] \tag{B.16}$$